Efficient parameter extraction in PV solar modules with the diligent crow search algorithm

Jabari, Mostafa; Nasab, Morteza Azimi; Zand, Mohammad; Tightiz, Lilia; Sanjeevikumar, Padmanaban; Vasquez, Juan C.

Published in:
Discover Energy

DOI (link to publication from Publisher):
10.1007/s43937-024-00063-3

Publication date:
2024

Document Version
Publisher's PDF, also known as Version of record

Discover Energy

Research

Efficient parameter extraction in PV solar modules with the diligent crow search algorithm

Mostafa Jabari[1] · Morteza Azimi Nasab[2] · Mohammad Zand[2] · Lilia Tightiz[3] · Sanjeevikumar Padmanaban[2] · Juan C. Vasquez Q[4]

Received: 6 July 2024 / Accepted: 18 December 2024
Published online: 29 December 2024

Abstract
In this study, we introduce a novel method that can be seamlessly integrated into existing metacognitive algorithms, significantly enhancing their performance during both exploitation and exploration phases. This method offers several advantages, including ease of implementation and simplicity in calculations, which collectively accelerate convergence to the global minimum and enhance the algorithm's robustness. Notably, it effectively avoids local minima, ensuring the algorithm does not become trapped. Furthermore, this method eliminates the need for developing new metacognitive algorithms. To demonstrate its benefits, we apply this method to the crow search optimization algorithm (CSA), which is notably deficient in convergence speed, robustness, stability, and escaping local minima. Consequently, the enhanced algorithm is termed the diligent crow search optimization algorithm (DCSA). Additionally, we utilize the powerful DCSA algorithm to identify the parameters of solar cells, aiming to maximize power output from solar energy—a critical global concern. To evaluate the proposed algorithm, we tested it on various solar cell models, including one-diode, two-diode, and three-diode configurations, as well as several widely used solar panels such as SM55, KC200GT, and SW255. We also examined the impacts of radiation, temperature, and unknown parameters on these solar panels. The simulation results demonstrate that implementing the proposed method on the crow algorithm resulted in a 98% improvement in stability and a sevenfold increase in convergence speed.

Keywords Photovoltaic · Optimization · Renewable energy · Crow search optimization algorithm

List of symbols

R_s	Series resistance (Ω)
R_{sh}	Shunt resistance (Ω)
I_{ph}	Current source (*Amp*)
I_t	Output current (*Amp*)
I_d	Diode current (*Amp*)
I_{sh}	Shunt resistance current (*Amp*)
I_{sd}	Diode reverse saturation current (*Amp*)
V_t	Terminal voltage (*V*)

✉ Sanjeevikumar Padmanaban, sanjeevi_12@yahoo.co.in; Mostafa Jabari, m_jabari97@sut.ac.ir; Morteza Azimi Nasab, morteza1368morteza@gmail.com; Mohammad Zand, dr.zand.mohammad@gmail.com; Lilia Tightiz, liliatightiz@gachon.ac.kr; Juan C. Vasquez Q, juq@et.aau.dk | [1]Faculty of Electrical Engineering, Sahand University of Technology Tabriz, Sahand, Iran. [2]Department of Electrical Engineering, Information Technology and Cybernetic, University of South-Eastern Norway, Notodden, Norway. [3]School of Computing, Gachon University, 1342 Seongnam-daero, Sujeong-Gu, Seongnam-Si 13120, Gyeonggi-Do, Korea. [4]Center of Reliable Power Electronics (CoRPE), Energy Engineering, Aalborg University, Aalborg, Denmark.

n	The diode ideality factor
q	The magnitude of charge on an electron (1.602×10^{-19})
k	The Boltzmann constant (1.381×10^{-23} (J/K))
T	The cell temperature (K)
g	Constant of gravity
u	Constant drift
$\widehat{e}_g$	Unity vector towards earth center
$\widehat{e}_w$	Unity vector in the wind direction
N	The number of grasshoppers
ub_d	The upper bound in the d-th dimension of $s(r)$
lb_d	The lower bound in the d-th dimension of $s(r)$
L	The maximum number of iterations
ep	Elimination percent
et	Elimination iteration
θ	Vector of unknown parameters
N_P	Number of solar cells in parallel
N_s	The number of solar cells in series
I_{ph_STC}	Light generated current at STC ($T_{STC} = 25°C$)
G	The surface irradiance of the cell (w/m^2)
G_{STC}	The irradiance at STC ($1000w/m^2$)
K_i	The short-circuit current coefficient
K_v	Open circuit voltage coefficient
N_E	The number of measured data
S_i	The social interaction
G_i	The gravity force on the grasshopper
A_i	Wind advection
d_{ij}	The distance between i-th and j-th grasshopper
$\widehat{d}_{ij}$	An unit vector from i-th to j-th grasshopper
$s(r)$	THE social forces strength
l	The attractive length scale
f	The attraction intensity
T_d	Value of the d-th dimension in the target
c_{max}	The maximum value of c
c_{min}	The minimum value of c
Th	Percentage of the problem domain
w	[0,1]

1 Introduction

The degradation of the environment and climate changes resulting from the extensive use of conventional fossil fuels like coal, oil, and gas, along with the gradual decline in valuable energy reservoirs, has increased the importance of adopting renewable energy sources. [1, 2]. Solar energy is one of the renewable and environmentally friendly energy sources [3], which in the direction of preserving clean air, public welfare, and valuable social comfort, is a highly valuable and entirely suitable alternative to fossil fuels. In line with harnessing abundant solar energy, photovoltaic technology in solar panels offers sustainable and environmentally-friendly solutions for electricity generation, emphasizing its pivotal role as a key alternative to prevalent fossil fuels.

Photovoltaic (PV) systems have numerous distinctive advantages, including straightforward installation, simple maintenance and repair, unlimited energy potential, noise-less operation, and the flexibility in system size [4]. Even with PV systems' broad appeal, it is crucial to remember that they still require thorough evaluations and analyses to pinpoint problems, lower total costs, and improve efficiency. Accurate modeling of the PV system as a whole and its components

has to receive a lot of attention after the early costs of setting up solar power networks [5]. To this end, the models used in PV systems are created to optimize the systems' efficiency by accurately estimating the energy generated [6].

The three primary categories of PV cell models—single diode (SDM), double diode (DDM), and triple diode (TDM) models [7]—each present their own set of challenges. The SDM, with its five unknown factors (current source, series resistance, shunt resistance, diode reverse saturation current, diode ideality factor), is often used to accurately depict the I-V characteristics. The DDM, with its seven unknown parameters, offers a more precise representation of a PV cell. According to various studies and the evaluation of different photovoltaic (PV) models for combined solar array and pumped hydro storage systems, the two-diode (TD) model, which accounts for recombination and other physical losses, is the most reliable and ecological. The TD model not only reduces the number of required PV panels and emissions but also ensures realistic system performance [8–11]. However, the extraction of these unknown characteristics and the differences in the extraction procedure from different PV models, including the TDM [12, 13], DDM [14–16], and SDM [17, 18], pose significant challenges. The nonlinear nature of I-V characteristics, potential inconsistency in solutions, fluctuations in environmental conditions, complexity of the model, inadequate data collection, potential mismatch between the model and real-world conditions, parameter interdependency, and sensitivity to input changes all contribute to the complexity of the modeling process [19]. This complexity should be seen as an intellectual challenge that researchers are uniquely positioned to tackle [20]. Meta-heuristic algorithms play a crucial role in the design and parameter identification of PV systems [21–23].

Meta-heuristic optimization algorithms have become increasingly popular as an attractive topic and a cost-effective approach to discover optimal solutions for complex problems. Population-based algorithms represent a highly prevalent class of meta-heuristic algorithms utilized worldwide. These algorithms work with a population of dynamic agents interacting locally with each other and their surroundings. Some of these methods are: Harris Hawkes optimization (HHO) [24], cat swarm optimization (CSO) [25], slime mould algorithm (SMA) [26], genetic algorithm (GA) [27], flower pollination algorithm (FPA) [28], gray wolf optimization (GWO) [17], bacterial foraging optimization (BFO) [29].

While classical optimization algorithms are effective in many scenarios, they also come with certain drawbacks. These methods often involve a high number of iterations and numerous particles, leading to limitations such as the potential for becoming trapped in local optima and lengthy convergence times required to reach the local minimum point [30]. The invention of new optimization methods and the development of optimization algorithms can partially answer the complex optimization problems and overcome these disadvantages [31].

These optimization methods are created from the combination of classical optimization methods. For example, flower pollination algorithm (FPA) [28] and gradient based optimizer (GBO) [32] face the limitation that they get stuck in local minima, hindering their ability to efficiently explore the entire search space. Conversely, some algorithms prioritize exploration and successfully identify a global minimum in the search space. However, they cannot reach the minimum global value. As seen in ant lion optimizer (ALO) [33] and bird mating optimizer (BMO) [34]. Realizing the need for a balanced integration of both exploration and exploitation phases, researchers propose algorithms that show more optimal performance overall. As a result, by integrating the two optimization methods, they succeed in introducing new optimization algorithms that have many advantages and few disadvantages in identifying PV module parameters, such as Boosted mutation-based Harris-hawk enhanced optimization (BHHO) [24].

Some methods focus on improving and addressing the drawbacks of population-based algorithms. Turbulent flow of water-based optimization algorithm (TFWO) [35], performance guided JAYA algorithm (PGJAYA) [34], enhanced Harris Hawks optimization (EHHO) [36], improved Lozi map based chaotic optimization Algorithm (ILCOA) [37], improved adaptive differential evolution (IADE) [38], flexible particle swarm optimization (FPSO) [39], modified salp swarm optimization (MSSA) [40], novel metaheuristic chaotic tunicate swarm algorithm (CTSA) [41], improved shuffled complex evolution algorithm (ISCE) [42], Whippy Harris Hawks Optimization (WHHO) [43], Springy Whale Optimization Algorithm (SWOA) [44], Repairable Grey Wolf Optimization algorithm (RGWO) [45], Improved Lozi Map based Chaotic Optimization Algorithm (ILCOA) [46] and so on [47–50]. Table 1 presents a compilation of various research studies conducted in recent years.

In addition to their numerous advantages and applications, optimization methods come with challenges such as identifying true optimal points, imprecision in parameter detection, the risk of getting stuck in local optima, long convergence time, and issues associated with fast convergence. These limitations drive researchers to explore alternative methods for parameter extraction from PV modules. After a thorough analysis of the Crow Search algorithm (CSA) [51] algorithm in 2017, it was found that there were deficiencies with significant weakness in exploration in both the exploitation and exploration phases.

In this paper, the DCSA is used to overcome the mentioned limitations of CSA and increase the efficiency of finding parameters and optimizing them in PV models. This research aims to minimize the disparity between experimental data and

Table 1 Summary of the optimization algorithms implemented in recent years

Refs.	Algorithm used	Model	Cost function	Compared methods	Achievement
[63]	COA	SDM DDM TDM	RMSE MAE	ABC, STBLO, OBWOA	Improved local and global search have been achieved
[64]	SMA	SDM DDM	RMSE	IJAYA, ERWCA, NMSOLMFO	Enhances the algorithm's capability for both exploration and exploitation
[65]	SFS	SDM DDM	RMSE	IJaya, HS, GA, IMFO, pSFS, BBO-M, NMSOLMFO	Improved local and global search have been achieved
[66]	DPDE	SDM DDM TDM	RMSE	DE, IJAYA, MLBSA, CLPSO, GWO, WDO	Robust and rapid strong convergence
[32]	CGBO	SDM DDM	RMSE	GBO, MPA, EO, IMO, WOA, PSO, IPSO	Incorporating chaotic behavior and fine-tuning the direction of movement leads to an enhanced convergence rate
[67]	ImSMA	SDM	RMSE	Diverse set of 19 algorithms	Robust and rapid strong convergence
[68]	GWOCSA	TDM	RMSE	PSO, MVO, SCA, CSA, GWO	The problem of premature convergence has been resolved
[69]	MSHOA	SDM DDM TDM	RMSE	PSO, GA, WOA, SFLA	Robust and rapid strong convergence
[70]	INFO	TDM	Combination of the absolute value of the current error	AEO, NGO, RCGA, CSA, RUN	Superior convergence time and accuracy in result

the proposed method by precisely determining the relevant variables associated with PV modules. This method has many advantages, such as not requiring complex calculations that can make the algorithm slower. The algorithm demonstrates exceptional convergence speed and efficiency in identifying the global optimal point, effectively avoiding local minima. It is crucial to emphasize that the performance evaluation of the SCSO algorithm involved its application to identify and extract unknown parameters from five solar modules: R.T.C France [52], PWP201 [53], SM55 [54], KC200GT [55], and SW255 [56]. Initially, the unknown parameters of various RTC France and PWP201 models were determined, followed by validation of the extracted parameters through comparison with experimental models under diverse temperature and radiation conditions. Furthermore, the impact of radiation and temperature on the parameters of these modules is elucidated and analyzed.

The contributions of this paper can be summarized as follows:

- Execution of the elimination phase: This phase includes the elimination of non-optimal solutions, such as the elimination of ineffective crows, and replacing them with new random crows. New solutions are strategically and regularly scattered in the search space to avoid getting stuck at local minima points.
- Search space control: instead of exploring the entire space in the problem, the proposed algorithm focuses on a limited part and occasionally expands it. This strategy provides acceptable efficiency and speed in searching the problem space.

In Sect. 2, we initially address the intricacies surrounding the PV cell and module model and elucidate the underlying internal dynamics. Following this, Sect. 3 introduces our new algorithm and provides a comprehensive explanation of its formulation and rationale. Moving forward, Sect. 4 begins with detailed simulations and analysis of the obtained data, elucidating the concrete implications of our method. Finally, Sect. 5 summarizes our key findings and their general significance and concludes the discussion. Using this structured methodology, we strive to provide a coherent and insightful exploration of the topic.

2 Mathematical modeling and problem formulation

2.1 PV cell model

Solar cells come in various configurations (single-diode model, double-diode model, triple-diode model), each with unique characteristics and applications. The single-diode model represents the basic operation of a solar cell with a single p–n junction. The double diode model includes an additional diode to account for recombination losses, providing a more accurate representation of the cell's behavior under different conditions. The triple diode model further refines this by incorporating additional parameters to capture more complex phenomena within the cell. Solar panels, composed of multiple interconnected solar cells, aggregate the electrical output to generate higher power levels suitable for practical applications.

Each of these models has unknown parameters that are crucial for accurate performance modeling. These parameters include the ideality factor, series resistance, shunt resistance, and photocurrent. Understanding the different types of solar cells and their unknown parameters is essential for developing precise mathematical models that describe their performance and optimize their efficiency.

2.1.1 Single-diode model

As can be seen from Fig. 1, the structure of this model consists of a diode, a series resistance (R_s), a shunt resistance (R_{sh}) and a current source (I_{ph}) [39]. Although the structure of this model is very simple, it is widely used in practice due to its proper accuracy of solar cell behavior. The output current (I_t) can be calculated as follows [41].

$$I_t = I_{ph} - I_{sh} - I_d \tag{1}$$

where I_{sh} and I_d denote shunt resistance current and the diode current, respectively. Their equations are as follow:

$$I_{sh} = \frac{V_t + I_t.R_s}{R_{sh}} \tag{2}$$

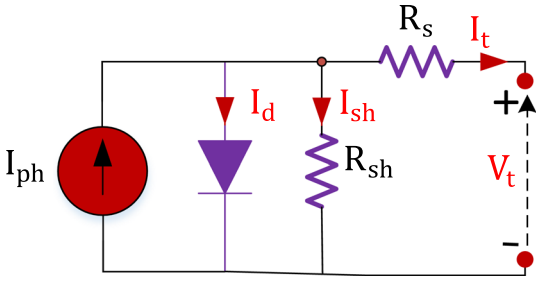

Fig. 1 Single diode model's equivalent circuit

$$I_d = I_{sd}\left[exp\left(\frac{q(V_t + R_s.I_t)}{n.k.T}\right) - 1\right] \tag{3}$$

In which, V_t is terminal voltage, I_{sd} is the diode reverse saturation current, n is the diode ideality factor, $q = 1.602 \times 10^{-19}$ is the magnitude of charge on an electron, $k = 1.381 \times 10^{-23}$ (J/K) is the Boltzmann constant and T is the cell temperature (K). Then, I_t can be rewritten as follows [40]:

$$I_t = I_{ph} - \frac{V_t + I_t.R_s}{R_{sh}} - I_{sd}\left[exp\left(\frac{q(V_t + R_s.I_t)}{n.k.T}\right) - 1\right] \tag{4}$$

From Eq. (4), it is clear that the five unknown parameters to be identified are:

$$\theta = \left[I_{ph}, R_s, R_{sh}, I_{sd}, n\right] \tag{5}$$

2.1.2 Double-diode model

Although SDM is considered an accurate model in engineering, researchers needed a more accurate model for specific applications. For this reason, they presented the double-diode model. In this model, as can be seen from Fig. 2, there is one more diode compared to SDM, which has led to the creation of 7 unknown parameters. The first diode is set as a rectifier and the second diode models the charge recombination current. The output current is obtained as follows:

$$I_t = I_{ph} - I_{sh} - I_{d_1} - I_{d_2} \tag{6}$$

As before, Eq. (6) can be rewritten using Eq. (2) and Eq. (3) as follows:

$$I_t = I_{ph} - \frac{V_t + I_t.R_s}{R_{sh}} - I_{sd_1}\left[exp\left(\frac{q(V_t + R_s.I_t)}{n_1.k.T}\right) - 1\right] - I_{sd_2}\left[exp\left(\frac{q(V_t + R_s.I_t)}{n_2.k.T}\right) - 1\right] \tag{7}$$

where $\left(I_{ph}, R_s, R_{sh}, I_{sd_1}, I_{sd_2}, n_1, n_2\right)$ are unknown parameters.

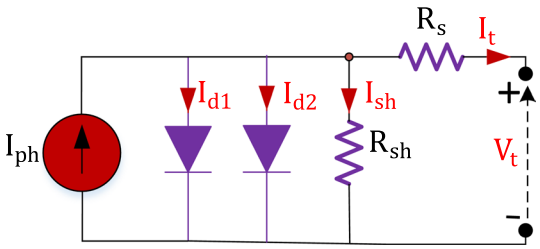

Fig. 2 Double diode model's equivalent circuit

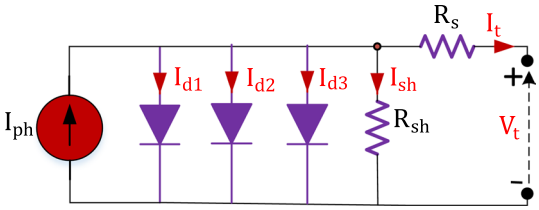

Fig. 3 Triple diode model's equivalent circuit

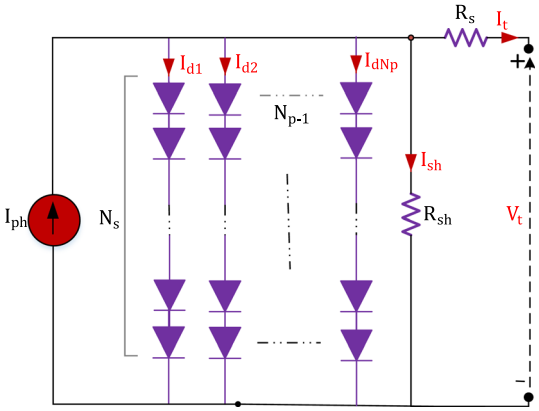

Fig. 4 PV model's equivalent circuit

2.1.3 Triple-diode model

The three-diode model, despite its increased accuracy compared to earlier models, sees limited practical application. This is due to its complexity, characterized by nine unknown parameters $\left(I_{ph}, R_s, R_{sh}, I_{sd_1}, I_{sd_2}, I_{sd_3}, n_1, n_2, n_3\right)$ which can pose a challenge for the suggested algorithm. As illustrated in Fig. 3, the computation of output current follows this procedure [42]:

$$I_t = I_{ph} - I_{sh} - I_{d_1} - I_{d_2} - I_{d_3} \tag{8}$$

Thus, the output current can be rewritten as follows:

$$I_t = I_{ph} - \frac{V_t + I_t.R_s}{R_{sh}} - I_{sd_1}\left[exp\left(\frac{q\left(V_t + R_s.I_t\right)}{n_1.k.T}\right) - 1\right] - I_{sd_2}\left[exp\left(\frac{q\left(V_t + R_s.I_t\right)}{n_2.k.T}\right) - 1\right] - I_{sd_3}\left[exp\left(\frac{q\left(V_t + R_s.I_t\right)}{n_3.k.T}\right) - 1\right] \tag{9}$$

2.1.4 PV module model

A PV module comprises multiple solar cells interconnected in series and/or parallel to create the single-diode PV module depicted in Fig. 4. The output current of this single-diode PV module can be determined using Eq. (10).

$$I_t = N_P.I_{ph} - \frac{N_P.V_t/N_s + I_t.R_s}{R_{sh}} - N_P.I_{sd}\left[exp\left(\frac{q\left(V_t/N_s + R_s.I_t/N_P\right)}{n.k.T}\right) - 1\right] \tag{10}$$

where N_P and N_s represent the number of solar cells in parallel and series, respectively. As elucidated in the introduction section, the performance of the solar cell system is contingent upon variations in temperature and irradiance. Therefore, to evaluate the system's performance under different temperature and irradiance conditions, it becomes imperative to reformulate the aforementioned equation utilizing the following equations:

$$I_{ph} = \left(I_{ph\_STC} + K_i \Delta T\right) \frac{G}{G_{STC}} \tag{11}$$

where, I_{ph_STC} (in Ampere) denotes the light-generated current at standard test conditions at STC,$\Delta T = T - T_{STC}$ (in Kelvin,$T_{STC} = 25°C$), G is the surface irradiance of the cell and G_{STC} ($1000w/m^2$) is the irradiance at STC. The constant K_i signifies the short-circuit current coefficient typically supplied by the manufacturer. An equation capturing the saturation current, which accounts for temperature fluctuations, is described by [39]:

$$I_{sd} = \frac{\left(I_{SC\_STC} + K_i \Delta T\right)}{\exp\left[\frac{q\left(V_{OC\_STC} + K_v \Delta T\right)}{n.k.T}\right] - 1} \tag{12}$$

The constant K_v is the open circuit voltage coefficient. This value is available from the datasheet.

2.2 Objective function

Figure 5 provides an overview of the solar module parameter identification process. As depicted, the output voltage and current, along with solar irradiance, are utilized as essential inputs to the PV cell model. Subsequently, the proposed algorithm endeavors to determine the unknown parameters of the system, aiming to reconcile the estimated current (I_{est}) with the actual output current. To achieve this objective, a cost function is required, defined as follows:

$$F(\theta) = RMSE(\theta) = \sqrt{\frac{1}{N_E} \sum_{i=1}^{N_E} f_M\left(V_t, I_t, \theta\right)^2} \tag{13}$$

where N_E represents the number of measured data and M is used for determining the SDM, DDM, TDM, and the PV panel. In Eq. 13, the function $f_M(V_t, I_t, \theta)$ represents the error between the estimated current (I_{est}) and the current measured (I_t) in the laboratory. Specifically, for the single diode model, the function $f_M(V_t, I_t, \theta)$ is derived by subtracting Eq. (4) from the measured current value (I_t), as shown in Eq. (14). Similarly, Eqs. (15) to (17) were obtained by using Eqs. (7), (9), and (10) respectively, instead of Eq. (4).

$$f_{SDM}\left(V_t, I_t, \theta\right) = \theta_1 - \frac{V_t + I_t.\theta_2}{\theta_3} - \theta_4 \left[exp\left(\frac{q\left(V_t + \theta_2.I_t\right)}{\theta_5.k.T}\right) - 1\right] - I_t \tag{14}$$

$$f_{DDM}\left(V_t, I_t, \theta\right) = \theta_1 - \frac{V_t + I_t.\theta_2}{\theta_3} - \theta_4 \left[exp\left(\frac{q\left(V_t + \theta_2.I_t\right)}{\theta_6.k.T}\right) - 1\right] - \theta_5 \left[exp\left(\frac{q\left(V_t + \theta_2.I_t\right)}{\theta_7.k.T}\right) - 1\right] - I_t \tag{15}$$

$$f_{DDM}\left(V_t, I_t, \theta\right) = \theta_1 - \frac{V_t + I_t.\theta_2}{\theta_3} - \theta_4 \left[exp\left(\frac{q\left(V_t + \theta_2.I_t\right)}{\theta_7.k.T}\right) - 1\right] - \theta_5 \left[exp\left(\frac{q\left(V_t + \theta_2.I_t\right)}{\theta_8.k.T}\right) - 1\right] - \theta_6 \left[exp\left(\frac{q\left(V_t + \theta_2.I_t\right)}{\theta_9.k.T}\right) - 1\right] - I_t \tag{16}$$

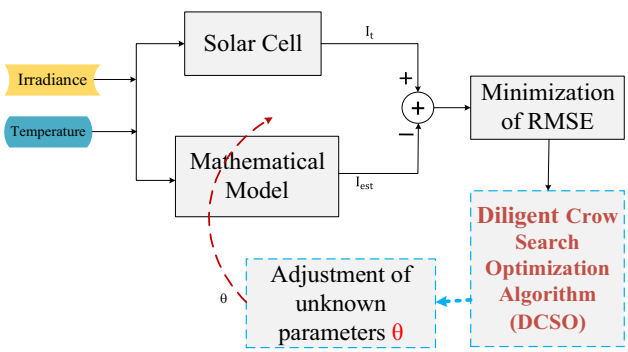

Fig. 5 Overview for parameters estimation of PV Cell models using DCSO

$$f_{panel}\left(V_t, I_t, \theta\right) = \theta_1 - \frac{V_t + I_t.\theta_2.N}{\theta_3.N} - \theta_4\left[exp\left(\frac{q\left(V_t + \theta_2.I_t.N\right)}{\theta_5.k.T.N}\right) - 1\right] - I_t \tag{17}$$

The unknown parameters vector is in the form of $\theta = [\theta_1, \theta_2, \theta_3, \theta_4, \theta_5]$ for the SDM and the PV panels, is in the form of $\theta = [\theta_1, \theta_2, \theta_3, \theta_4, \theta_5, \theta_6, \theta_7]$ for the DDM and is in the form of $\theta = [\theta_1, \theta_2, \theta_3, \theta_4, \theta_5, \theta_6, \theta_7, \theta_8, \theta_9]$ for the TDM.

3 Crow search algorithm

Crows are recognized as remarkably intelligent avian species owing to their relatively large brain size in proportion to their body. They exhibit a wide array of intelligent behaviors, including self-awareness, tool creation, facial recognition, and the capacity to communicate and retain knowledge of food cache locations for extended periods. Crows engage in the observation and pilfering of sustenance from other birds, while concurrently employing preventative measures to avoid becoming prey themselves. As a result of their collective behavior, memory retention, coordinated theft tactics, and protection of valuable resources, the crow search algorithm has emerged as a metaheuristic algorithm inspired by these intelligent attributes observed in crow populations [57].

Crows have a memory where they remember the location of their hiding place ($m^{i,iter}$). At each iteration, each crow has a position in their memory which represents their best hiding place found so far. Crows move in the environment (the search space) and search for better hiding places. If at a certain iteration, one crow decides to follow another crow to its hiding place, there are two possible scenarios. In the first state, the followed crow (j) is not aware of being followed and the following crow (i) will approach its hiding place. The new position of the following crow is determined using a specific method.

In State 2, Crow j is aware that Crow i is following it. To prevent Crow i from stealing its cache, Crow j will deceive Crow i by moving to a different location in the search space. States 1 and 2 can be summarized as the awareness of Crow j about Crow i's presence and its strategy to mislead crow i [57].

$$x^{i,iter+1} = \begin{cases} x^{i,iter} + r_i \times fl^{i,iter} \times \left(m^{j,iter} - x^{i,iter}\right) r_j \geq AP^{j,iter} \\ \textit{a random position otherwise} \end{cases} \tag{18}$$

where $x^{i,iter}$ is the position of crow i at time (iteration) $iter$ in the search space, r_i, r_j is a random number [0,1], $fl^{i,iter}$ illustrates the flight length of crow i at $iter$ and $AP^{j,iter}$ denotes the awareness probability of crow j at $iter$.

3.1 Diligent crow search algorithm

The accuracy of the information provided in the corresponding articles regarding the drawbacks of the algorithm has been substantiated through thorough reviews and tests performed on the Crow Search algorithm, specifically for its optimization applications. Among the noteworthy limitations are the algorithm's sluggish convergence rate, limited capability to identify numerous unexplored system parameters, and the tendency to become trapped in local optima. In order to address these shortcomings, we have introduced the DCSA.

The DCSA incorporates simple yet highly efficient strategies. The initial approach involves removing a set of underperforming Crows (the least effective approach) during each iteration and randomly dispersing new Crows in previously unexplored areas of the search space. As a result, a well-balanced combination of exploitation and exploration is achieved. Moreover, this process involves the inclusion of supplementary parameters (et, ep, Th, w) in the CSA. The modifications made to the CSA algorithm are depicted in green in Fig. 6, which represents the flowchart of the proposed algorithm.

To achieve a balance between exploration and exploitation, new design factors have been implemented. This method keeps the overall crow population constant and computes the objective function value for each crow after a predefined number of rounds. Then, some of the least active crows—which stand for subpar solutions—are eliminated and replaced with fresh crows that are inserted at random into the search area. To put this strategy into perspective, the best solution for the Rastrigin function is found by applying the DCSA (see Fig. 7).

The search space spans from -5.12 to 5.12, while the following parameters were carefully selected: a total of 100 iterations, a population size of 20 Crows, 20 elimination process (ep), and 50 iterations for replacement (et). Figure 7a provides a comprehensive 3D representation of the Rastrigen function, showcasing numerous local minimum and maximum

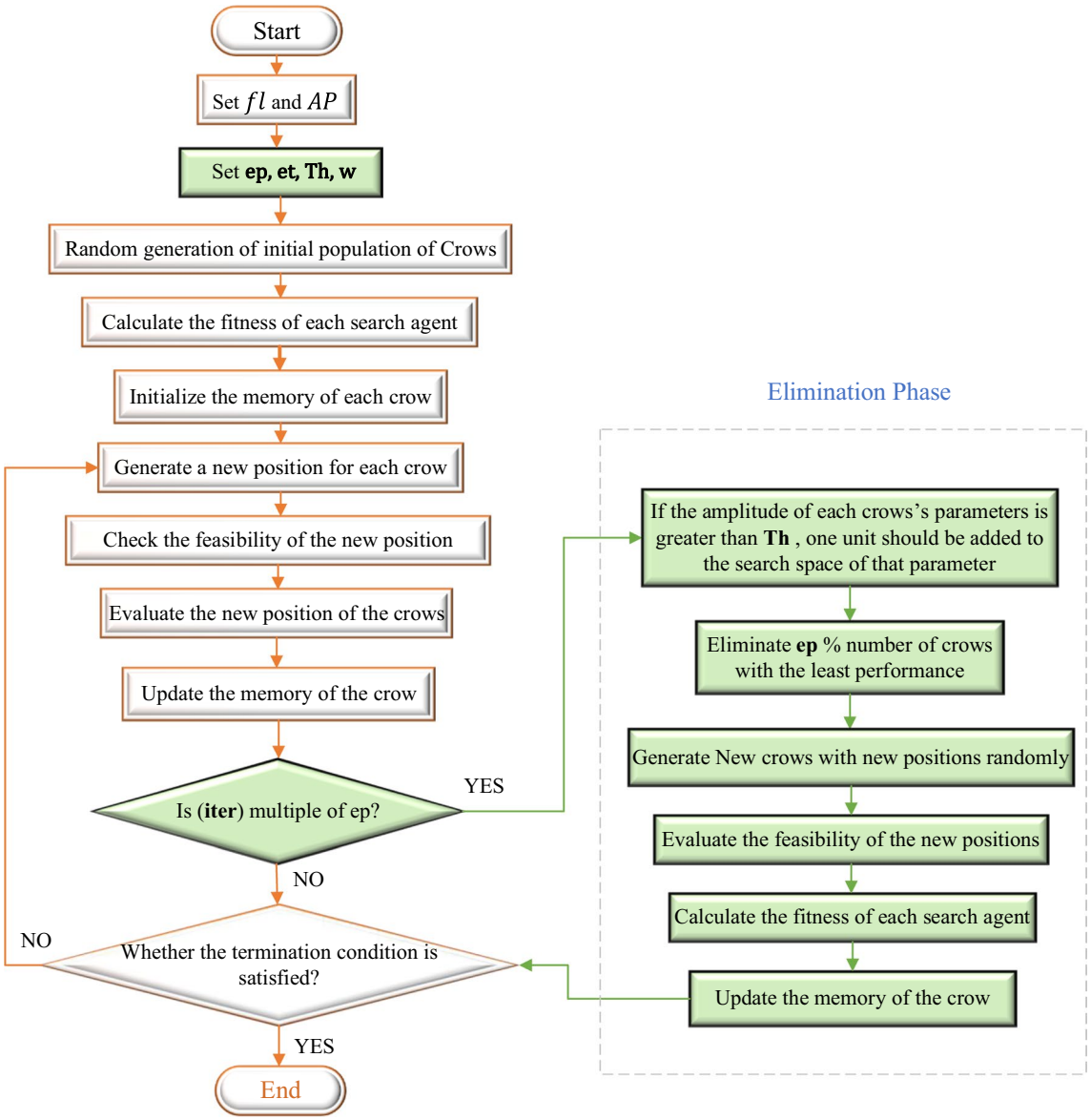

Fig. 6 Flowchart of DCSA algorithm

points highlighted in blue and yellow respectively. Worth mentioning is the existence of a solitary global minimum point at coordinates [0,0] within the Rastrigen function. Nevertheless, to effectively demonstrate the efficacy of the proposed algorithm, a two-dimensional depiction of the Rastrigen function has been employed. It is noteworthy that the algorithm refrains from entering the elimination loop until the 19th iteration, with the crows becoming trapped in the local minimum at [2,−1]. By imposing the condition of entering the elimination loop (ep = 20), the algorithm expels et = 50% of the crows that have obtained inferior solutions compared to the remaining crows, and replaces them randomly within the search space. Evidently, as illustrated in Fig. 7c, two crows are randomly positioned in the global minimum, inducing the other crows to abandon the local minimum and navigate towards them.

The second concept aims to enhance the accuracy of algorithms in finding the best answer (global minimum) by effectively controlling the search space. This is achieved through the utilization of *Th* and *w* parameters. Initially, Crows conduct searches within a limited search space. However, once a certain criterion is fulfilled (e.g. a predetermined percentage of the maximum iteration), the search space expands at a rate of *w*. This expansion process continues until the entire search space is explored. An additional advantage of this approach is its ability to achieve optimal solutions with fewer Crows, eliminating the need for a large number as required in the CSA algorithm. Consequently, the execution

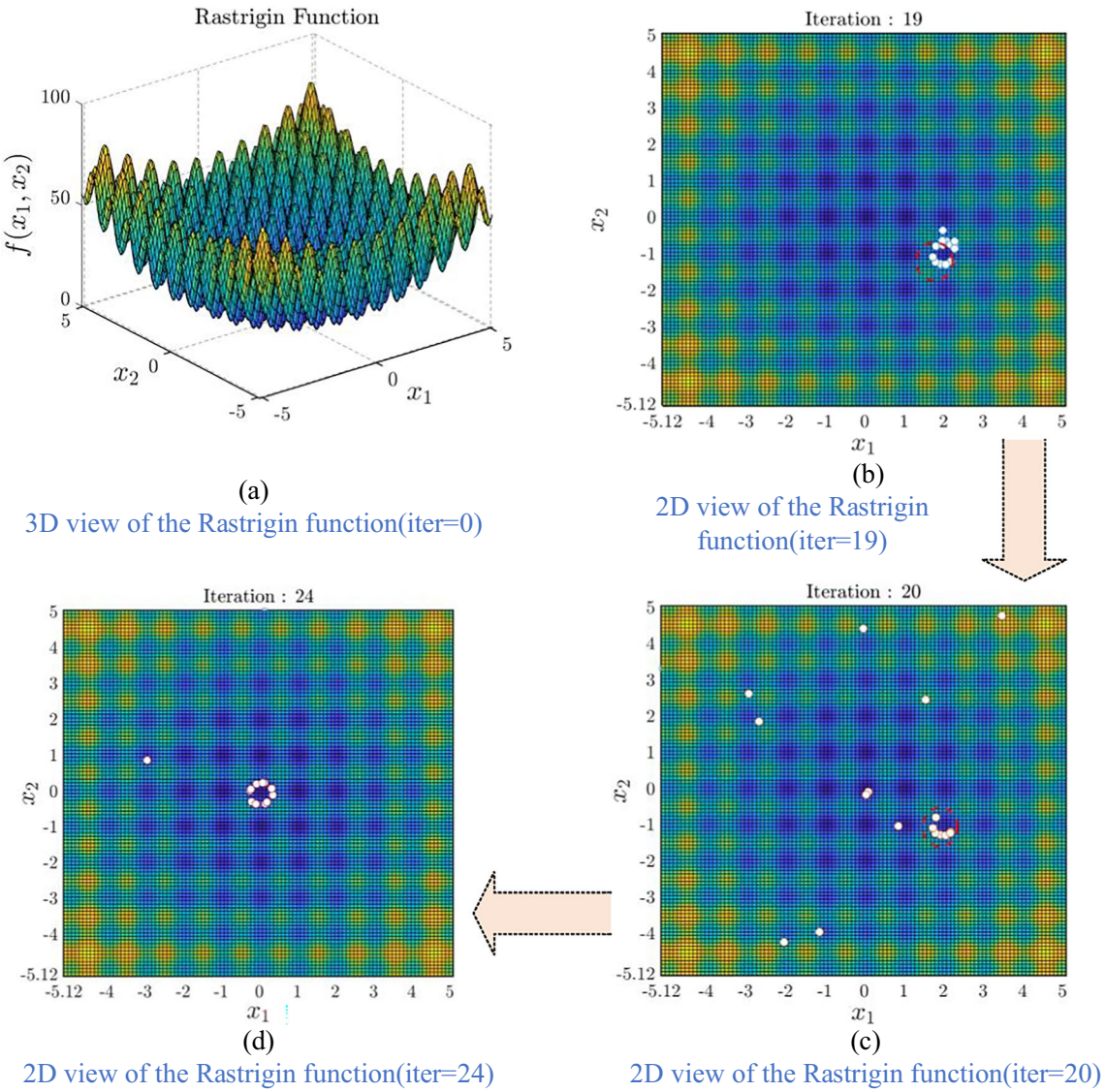

Fig. 7 Found the minimum value of the Rastrigen function by DCSA, **a** before eliminate phase[3D view and iteration = 0], **b** before eliminate phase[2D view and iteration = 19], **c** After eliminate phase[2D view and iteration = 20], **d** After eliminate phase[2D view and iteration = 24]

time of the algorithm is significantly reduced compared to the classic CSA algorithm, resulting in faster convergence towards the global solution.

4 Simulations

This section evaluates the performance of the DCSA algorithm by determining the unknown parameters of several widely used solar systems in the industry. In particular, the French R.T.C system with a diameter of 57 mm, the Photowatt-PWP201 system including 36 polycrystalline solar cells, as well as the SM55 (monocrystalline), KC200GT (multicrystalline) and SW255 (polycrystalline) systems were identified. These systems were tested under different conditions of radiation and temperature with the specifications presented in Table 2.

Initially, unknown parameters of RTC France and PWP201 systems were identified in all models: single diode, two diodes and three diodes. After that, the effect of radiation and temperature on SM55, KC200GT and SW255 modules was investigated in the next section. Table 3 shows the search space for unknown parameters.

Table 2 Experimental data of the examined modules at STC

Parameters	SM55	KC200GT	SW255
Maximum power ($P_{max}(W)$)	55	200	255
Voltage at P_{max} ($V_{ppm}(V)$)	17.4	26.3	31.4
Current at P_{max} ($I_{ppm}(A)$)	3.15	7.61	8.15
Open circuit voltage ($V_{oc}(V)$)	21.7	32.9	37.8
Short circuit Current ($I_{sc}(A)$)	3.45	8.21	8.66
K_V (mV/°C)	−76	−123	−30
K_I (mA/°C)	1.40	3.18	4
Number of cells	36	54	60

Table 3 Ranges of parameters for PV modules

Parameter	RTC France PV		PWP201		PV module	
	Minimum limit	Maximum limit	Minimum limit	Maximum limit	Minimum limit	Maximum limit
$I_{ph}(A)$	0	1	0	2	0	$2I_{SC}$
$I_{sd}, I_{sd2}, I_{sd3}(\mu A)$	0	1	0	50	0	100
$R_s(\Omega)$	0	0.5	0	2	0	2
$R_{sh}(\Omega)$	0	100	0	1000	0	5000
n_1, n_2	1	2	1	50	1	4
n_3	2	5	1	50		

Furthermore, 12 metaheuristic algorithms are compared in addition to the DCSA algorithm. To ensure a comprehensive and unbiased comparison, the selected algorithms include the latest algorithms, such as FPSO, WHHO, and SWOA, along with well-known algorithms, such as GA and PSO. For all systems, a fixed number of iterations (5000) is employed, and the parameters of each algorithm are chosen and adjusted based on pertinent references to maximize their performance. Simulations were conducted using the MATLAB 2020b environment.

4.1 Parameters identification of R.T.C France solar cell

RTC France is a widely used solar module that is often mentioned in the scientific literature. Table 4 presents a comprehensive data set including the measured voltage and current values of the RTC module used to determine the unknown parameters. The next columns in this table show the current estimated by the proposed algorithm in three single diode, two diode and three diode models. The relative error is expressed as follows [39]:

$$R_{err} = \frac{I_t - I_{est}}{I_{est}} \tag{19}$$

Table 4 shows that the relative error is remarkably low and shows a close similarity between the estimated and measured current values. In addition, a careful examination of this table shows that the error value in the three-diode model is lower than that of the single-diode model and shows the superior accuracy of the three-diode model. Indeed, the TD model not only minimizes the number of required PV panels and emissions but also guarantees realistic system performance [10].

Table 5 lists the values of the unknown parameters identified by the DCSA algorithm and 12 alternative algorithms. It is clear from the table that similar to the DCSA algorithm, half of the used algorithms obtained the lowest root mean square error value. As a result, for further investigation, we compare the convergence speed of these algorithms with the proposed algorithm (see Fig. 8). From this figure, it is obvious that the DCSA algorithm shows the fastest convergence speed, while the CSA algorithm initially encounters a local minimum, which shows the slowest convergence speed. To better evaluate the performance of the algorithms during the initial iterations, the results have been zoomed in from iteration 30 to iteration 70. As illustrated, the WHHO and RGWO algorithms rapidly approached the minimum value but

Table 4 Relative error for each measurement

DATA	$V_L(v)$	$I_L(A)$	SDM		DDM		TDM	
			$I_{te}(A)$	R_{err}	$I_{te}(A)$	R_{err}	$I_{te}(A)$	R_{err}
1	−0.2057	0.7640	0.76408762	−0.00011467	0.76400689	−0.00000902	0.76397499	0.00003272
2	−0.1291	0.7620	0.76266262	−0.00086882	0.76261742	−0.00080960	0.76259970	−0.00078639
3	−0.0588	0.7605	0.76135471	−0.00112262	0.76134196	−0.00110589	0.76133709	−0.00109950
4	0.0057	0.7605	0.76015421	0.00045488	0.76017078	0.00043308	0.76017726	0.00042454
5	0.0646	0.7600	0.75905584	0.00124385	0.75909801	0.00118823	0.75911400	0.00116714
6	0.1185	0.7590	0.75804300	0.00126245	0.75810599	0.00117925	0.75812906	0.00114878
7	0.1678	0.7570	0.75709158	−0.00012097	0.75716851	−0.00022256	0.75719531	−0.00025794
8	0.2132	0.7570	0.75614206	0.00113461	0.75622294	0.00102754	0.75624883	0.00099328
9	0.2545	0.7555	0.75508732	0.00054652	0.75515856	0.00045213	0.75517733	0.00042727
10	0.2924	0.7540	0.75366447	0.00044519	0.75371010	0.00038462	0.75371342	0.00038022
11	0.3269	0.7505	0.75138806	−0.00118189	0.75139349	−0.00118911	0.75137000	−0.00115789
12	0.3585	0.7465	0.74734835	−0.00113514	0.74730576	−0.00107823	0.74723818	−0.00098789
13	0.3873	0.7385	0.74009688	−0.00215767	0.74001189	−0.00204306	0.73987231	−0.00185479
14	0.4137	0.7280	0.72739678	0.00082927	0.72729093	0.00097493	0.72703227	0.00133105
15	0.4373	0.7065	0.70695328	−0.00064117	0.70685917	−0.00050813	0.70641266	0.00012363
16	0.4590	0.6755	0.67529490	0.00030371	0.67524303	0.00038055	0.67450718	0.00147190
17	0.4784	0.6320	0.63088431	0.00176844	0.63088692	0.00176429	0.62975018	0.00357254
18	0.4960	0.5730	0.57208207	0.00160453	0.57212854	0.00152317	0.57047793	0.00442097
19	0.5119	0.4990	0.49949164	−0.00098429	0.49955470	−0.00111039	0.49730485	0.00340866
20	0.5265	0.4130	0.41349356	−0.00119363	0.41354371	−0.00131476	0.41063884	0.00574996
21	0.5398	0.3165	0.31721949	−0.00226814	0.31723756	−0.00232495	0.31366883	0.00902597
22	0.5521	0.2120	0.21210317	−0.00048641	0.21208588	−0.00040494	0.20786978	0.01986923
23	0.5633	0.1035	0.10272134	0.00758021	0.10268161	0.00797015	0.09786862	0.05754013
24	0.5736	−0.0100	−0.00924885	0.08121534	−0.00928748	0.07671735	−0.01464024	−0.31695138
25	0.5833	−0.1230	−0.12438135	−0.01110582	−0.12438858	−0.01116327	−0.13023079	−0.05552291
26	0.5900	−0.2100	−0.20919307	0.00385732	−0.20915624	0.00403409	−0.21532151	−0.02471428

Table 5 Detailed results for SDM of RTC France

Algorithms	$I_{ph}(A)$	$I_{sd}(\mu A)$	n	$R_s(\Omega)$	$R_{sh}(\Omega)$	RMSE
DCSA	0.76077551	0.32302069	1.48110820	0.03637709	53.71865806	**9.86021877e-04**
CSA	0.76076804	0.32377032	1.481341280	0.03636755	53.82556489	9.86038185e-04
LGOA	0.760891	0.338992	1.4861	0.0361998	53.2146	1.0944e-3
FPSO	0.7607	0.3230	1.4811	0.03637	53.7185	**9.8602e-4**
WHHO	0.76077551	0.3230231	1.48110808	0.03637710	53.71867407	**9.8602e-4**
SWOA	0.76077551	0.32302318	1.48110897	0.03637706	53.71886754	**9.8602e-4**
RGWO	0.76077553	0.323020823	1.48118359	0.03637709	53.7185261	**9.8602e-4**
ILCOA	0.760775	0.323021	1.481108	0.036377	53.718679	**9.86021e-4**
EHHO[43]	0.760775	0.323	1.481238	0.036375	53.74282	**9.8602e-4**
WOA	0.76075413	0.3243611	1.4815199	0.03636524	54.10454052	9.8615e-4
LCOA[37]	0.760752	0.323278	1.481187	0.036374	53.902365	9.86094e-4
PSO	0.7607	0.400	1.5033	0.0354	59.012	1.38e-03
GA	0.7619	0.8087	1.5751	0.0299	42.3729	1.8704e-02

Bold numbers are the best optimal answers

remained trapped in the local minimum for an extended period. In contrast, the proposed algorithm successfully navigated past the local minima with ease.

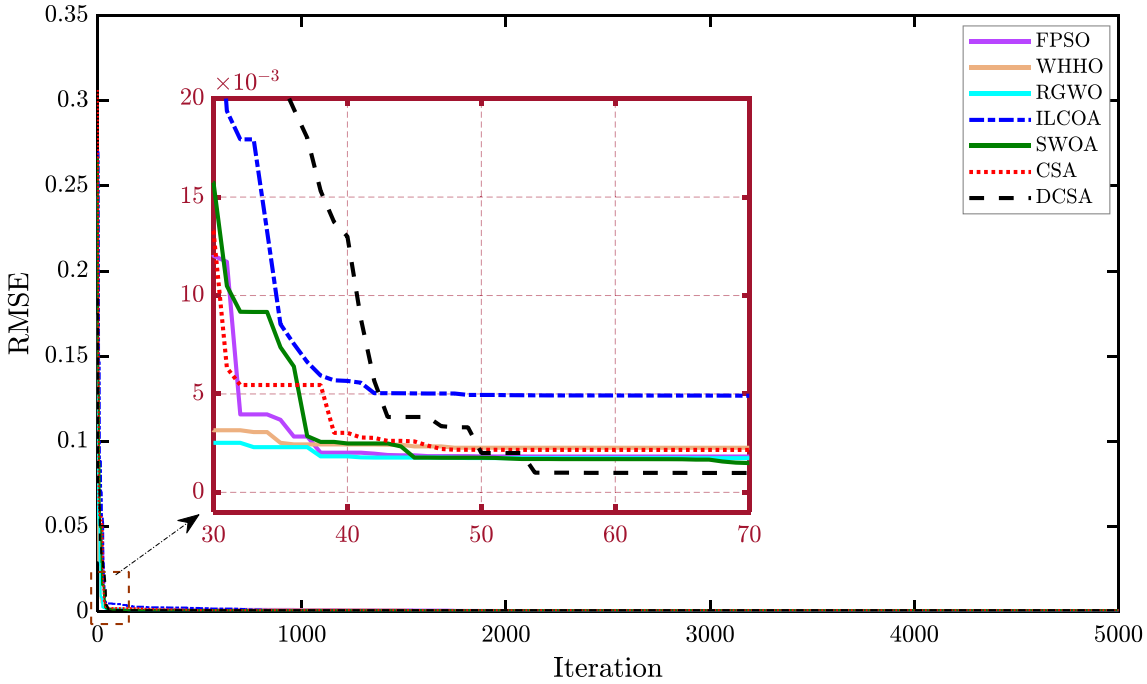

Fig. 8 Analysis of RMSE for algorithms in single diode model

Table 6 Detailed results for DDM of RTC France

Algorithms	$I_{ph}(A)$	$I_{sd1}(\mu A)$	$I_{sd2}(\mu A)$	n_1	n_2	$R_s(\Omega)$	$R_{sh}(\Omega)$	RMSE
DCSA	0.76078102	0.24174052	0.59361297	1.45664101	1.99055222	0.03666774	55.09532608	**9.82477e-04**
CSA	0.76077099	0.23870616	0.58689023	1.45572496	1.97569113	0.03667121	55.34360036	9.8287e-04
LGOA	0.76077	0.21	0.21	1.4497	1.6745	0.03666	55.2016	9.9691e-4
FPSO	0.76078	0.22731	0.72786	1.45160	1.99969	0.036737	55.3923	9.8253e-04
WHHO	0.76078	0.22857	0.72718	1.45189	2	0.03672	55.42643	9.82487e-04
SWOA	0.76078	0.70757	0.23082	2	1.452711	0.036719	55.371095	9.8249e-04
RGWO	0.76078	0.22718	0.74714	1.45144	0.760781	0.03672	55.54442	9.82511e-04
ILCOA	0.76078	0.22601	0.74921	1.45101	2.00000	0.036739	55.5320	9.8257e-04
EHHO	0.76076	0.58618	0.24096	1.968451	1.4569104	0.0365988	55.6394395	9.83606e-04
WOA	0.76077	0.26185	0.22162	1.4645250	1.82539530	0.0365306	54.3404740	9.8464e-04
LCOA	0.76077	0.26612	0.38023	1.46205	1.9938	0.3667	54.6314	9.8423e-4
PSO	0.7623	0.4767	0.0102	1.5172	2	0.0325	43.1034	1.6600e-03
GA	0.7608	0.0001	0.0001	1.3355	1.481	0.0364	53.7185	3.6040e-01

Bold numbers are the best optimal answers

The values of the unknown parameters for the two-diode and three-diode models are displayed in Tables 6 and 7, respectively. Compared to the single-diode model, these models have more unknown parameters, which makes them more difficult for algorithms to solve. However, the DCSA method had the lowest RMSE value, followed by the WHHO and DCSA algorithms, demonstrating its effectiveness despite the increased complexity. Figures 9 and 10 show the convergence speed of the algorithms for the two- and three-diode models, respectively. These graphs show that the suggested approach has the fastest convergence rate. The resistance and stability of the algorithms are assessed after the convergence speed evaluation. Every algorithm underwent thirty iterations, with the outcomes compiled in Table 8. The table illustrates that in single and double diode models, the DCSA algorithm demonstrates a very favorable resistance and attains the lowest value within 30 iterations. Notably, the three-diode model likewise has remarkable stability. Upon closer examination, it is evident that some algorithms, such as SWOA and RGWO, exhibit superior initial speed compared to the proposed algorithm. However, they fail to sustain this speed and avoid getting

Table 7 Detailed results for TDM of RTC France

Algorithms	$I_{ph}(A)$	$I_{sd1}(\mu A)$	$I_{sd2}(\mu A)$	$I_{sd3}(\mu A)$	n_1	n_2	n_3	$R_s(\Omega)$	$R_{sh}(\Omega)$	RMSE
DCSA	0.76078249	0.23822262	0.45263548	0.80000000	1.45363421	2	2.41341536	0.03672833	55.66795697	**9.80251928e-04**
CSA	0.76078138	0.22105681	0.65925819	0.50698498	1.44754319	2	2.38937217	0.03679762	55.85266253	9.81475349e-04
LGOA	0.760781	0.22842	0.57977	0.5851	1.45129	2	2.38495	0.03176	55.78076	9.81148e-04
FPSO	0.7607	0.2225	0.7467	0.2353	1.4495	2	2.5851	0.0367	55.7531	9.8203e-04
WHHO	0.76078	0.23910	0.43972	0.8	1.45393	2	2.40415	0.03672	55.64995	9.80751e-04
SWOA	0.76078	0.24204	0.36359	1	1.45602	2	2.40819	0.03672	55.69461	9.8033e-04
RGWO	0.76078	0.49872	0.23049	0.67753	1.99999	1.45090	2.32581	0.03675	55.78999	9.81064e-04
ILCOA	0.7607	0.2231	0.7390	0.2226	1.4497	2	2.5771	0.0367	55.6554	9.8204e-04
EHHO	0.76078	0.22854	0.57999	0.5861	1.45029	2	2.39655	0.03676	55.77064	9.81232e-04
WOA	0.76077	0.2353	0.2213	0.4573	1.4543	1.4978	2	0.03668	55.4448	9.8249 e-04
LCOA	0.76078	0.22844	0.57979	0.5858	1.44929	2	2.39450	0.03471	55.78074	9.81754e-04
PSO	0.7607	0.2259	0.7491	0.0023	1.4509	2	2.3156	0.0367	55.47571	9.8247e − 04
GA	0.7605	0.3251	0.3608	0	1.4843	1.9975	2.2099	0.0357	58.6086	1.0531e − 03

Bold numbers are the best optimal answers

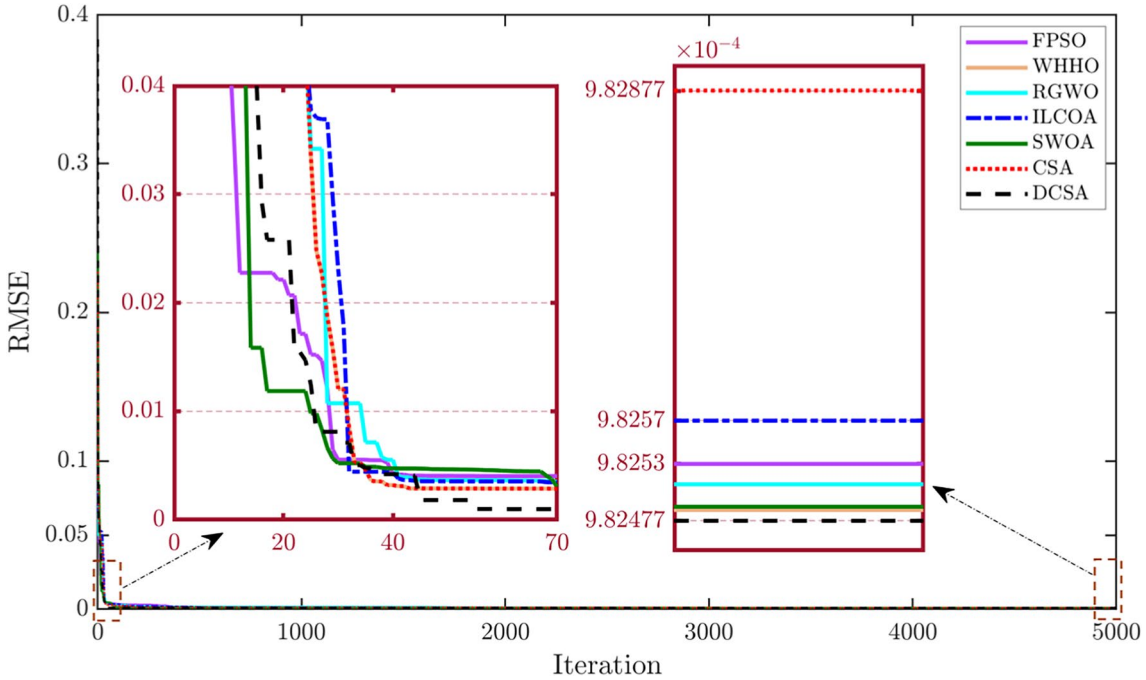

Fig. 9 Analysis of RMSE for algorithms in double diode model

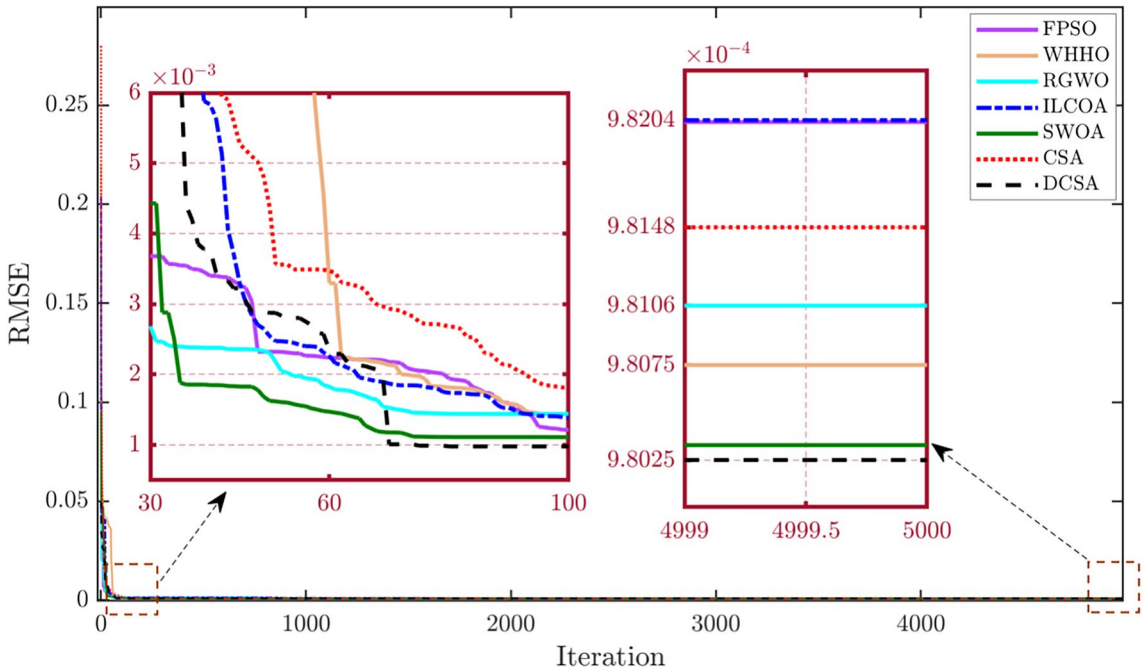

Fig. 10 Analysis of RMSE for algorithms in triple diode model

trapped in local minima. In contrast, the proposed algorithm consistently maintains its high speed, successfully bypasses local minima, and ultimately reaches the global minimum.

4.2 Parameters identification of photowatt-PWP201 PV module

Table 9 displays the PWP201 module's measured voltage and current in the second and third columns, a commercial PV module with 36 polycrystalline cells. The remaining columns show the current detected by the suggested

Table 8 Comparative evaluation of RMSE for SDM, DDM, and TDM of RTC France through different methodologies over 30 runs

Algorithm	DCSA	CSA	LGOA	FPSO	WHHO	SWOA	RGWO	ILCOA	EHHO	WOA	LCOA	PSO	GA
SDM													
Min	**9.860218e-4**	9.8603e-04	1.0944e-03	**9.8602e-04**	**9.8602e-04**	**9.8602e-04**	**9.8602e-04**	**9.860218e-04**	**9.8602e-04**	9.8615e-04	9.860945e-04	1.38e-03	1.8704e-02
Mean	**9.860218e-4**	9.8884e-04	1.8110e-03	**9.8602e-04**	**9.8602e-04**	**9.8602e-04**	**9.8602e-04**	9.8839e-04	9.8645e-04	9.8621e-04	9.9421e-04	1.4161e-03	1.9903e-02
Max	**9.860218e-4**	9.8964e-04	3.0010e-03	**9.8602e-04**	**9.8602e-04**	**9.8602e-04**	**9.8602e-04**	9.9484e-04	9.8862e-04	9.8798e-04	9.9821e-04	1.5123e-03	2.5146e-02
DDM													
Min	**9.82477e-04**	9.8287e-04	9.9691e-04	9.8253e-04	9.82487e-04	9.8249e-04	9.82511e-04	9.8257e-04	9.83606e-04	9.8464e-04	9.8423e-04	1.6600e-03	3.6040e-01
Mean	9.82479e-04	9.9467e-04	1.6541e-03	9.8331e-04	9.8315e-04	9.8250e-04	9.8356e-04	9.8258e-04	9.83606e-04	9.8651e-04	9.8561e-04	1.7463e-03	3.6497e-01
Max	9.82487e-04	1.0451e-03	1.9845e-03	1.8476e-03	9.8324e-04	9.8261e-04	9.8412e-04	9.8264e-04	9.83606e-04	9.8741e-04	9.8562e-04	1.9476e-03	1.0010
TDM													
Min	**9.8025e-04**	9.8147e-04	9.81148e-04	9.8203e-04	9.80751e-04	9.8033e-04	9.81064e-04	9.8204e-04	9.81232e-04	9.8249 e-04	9.81754e-04	9.8247e-04	1.0531e-03
Mean	9.8030e-04	9.9584e-04	9.8254e-04	9.8206e-04	9.8077e-04	9.8034e-04	9.8106e-04	9.8379e-04	9.8461e-04	9.8264e-04	9.8652e-04	9.8364e-04	1.8496e-03
Max	9.8051e-04	9.9794e-04	9.8252e-04	9.8208e-04	9.8100e-04	9.8036e-04	9.8106e-04	9.8997e-04	9.8514e-04	9.8401e-04	9.9546e-04	9.9431e-04	2.6478e-03

Bold numbers are the best optimal answers

Table 9 Relative error for each measurement

DATA	$V_L(v)$	$I_L(A)$	SDM		DDM		TDM	
			$I_{te}(A)$	R_{err}	$I_{te}(A)$	R_{err}	$I_{te}(A)$	R_{err}
1	0.1248	1.0315	1.02912208	0.00231062	1.03181587	−0.00030613	1.03136248	0.00013333
2	1.8093	1.0300	1.02738434	0.00254593	1.03051478	−0.00049953	1.02994785	0.00005063
3	3.3511	1.0260	1.02574213	0.00025139	1.02715634	−0.00112576	1.02591347	0.00008434
4	4.7622	1.0220	1.02410399	−0.00205447	1.02224178	−0.00023651	1.02286262	−0.00084333
5	6.0538	1.0180	1.02228341	−0.00419004	1.01784163	0.00015559	1.01859517	−0.00058430
6	7.2364	1.0155	1.01991740	−0.00433114	1.01456797	0.00091864	1.01513647	0.00035810
7	8.3189	1.0140	1.01635082	−0.00231300	1.01434789	−0.00034296	1.01356269	0.00043145
8	9.3097	1.0100	1.01049143	−0.00048633	1.01113479	−0.00112229	1.01095674	−0.00094637
9	10.2163	1.0035	1.00067876	0.00281931	1.00309471	0.00040403	1.00303438	0.00046421
10	11.0449	0.9880	0.98465335	0.00339880	0.98788945	0.00011190	0.98784121	0.00016074
11	11.8018	0.9630	0.95969740	0.00344128	0.95679134	0.00648904	0.96399759	−0.00103484
12	12.4929	0.9255	0.92304875	0.00265560	0.92497624	0.00056624	0.92505884	0.00047689
13	13.1231	0.8725	0.87258815	−0.00010102	0.87312647	−0.00071750	0.87306479	−0.00064690
14	13.6983	0.8075	0.80731011	0.00023520	0.80698476	0.00063847	0.80705464	0.00055183
15	14.2221	0.7265	0.72795781	−0.00200260	0.72612347	0.00051854	0.72636719	0.00018284
16	14.6995	0.6345	0.63646617	−0.00308920	0.63473149	−0.00036470	0.63411147	0.00061271
17	15.1346	0.5345	0.53569606	−0.00223273	0.53421796	0.00052794	0.53467941	−0.00033554
18	15.5311	0.4275	0.42881614	−0.00306926	0.42796118	−0.00107762	0.42703476	0.00108946
19	15.8929	0.3185	0.31866865	−0.00052926	0.31776429	0.00231526	0.31837164	0.00040317
20	16.2229	0.2085	0.20785711	0.00309290	0.20899567	−0.00237167	0.20889766	−0.00190361
21	16.5241	0.1010	0.09835421	0.02690058	0.10149746	−0.00490120	0.10179413	−0.00780133
22	16.7987	−0.0080	−0.00816933	−0.02072813	−0.00799466	0.00066794	−0.00846177	−0.05457132
23	17.0499	−0.1110	−0.11096845	0.00028423	−0.11403578	−0.02662129	−0.11162014	−0.00555580
24	17.2793	−0.2090	−0.20911761	−0.00056244	−0.20883456	0.00079220	−0.20946791	−0.00223380
25	17.4885	−0.3030	−0.30202238	0.00323691	−0.30333479	−0.00110369	−0.30279463	0.00067824

Table 10 Detailed results for SDM of PWP201

Algorithm	$I_{ph}(A)$	$I_{sd1}(\mu A)$	$R_s(\Omega)$	$R_{sh}(\Omega)$	n_1	RMSE
DCSA	1.03051428	3.48227120e-06	1.20127077	981.98498435	1.3499925	**2.42507186e-03**
CSA	1.04886249	3.57803151e-06	1.17022543	330.63439619	1.35429618	6.43769589e-03
FPSO	1.03061	3.45162	1.20206	966.77093	1.34906	2.42525e-03
WHHO	1.03051	3.48210	1.20127	981.90523	1.34998	**2.42507e-03**
EHHO	1.03058	3.45996	1.20185	971.27602	1.34931	2.42516e-03
SWOA	1.03051	3.48221	1.20127	981.96750	1.34999	**2.42507e-03**
CWOA	1.03164	3.09598	1.21219	827.54687	1.33768	2.45168e-03
WOA	1.03393	2.49034	1.23192	644.59884	1.31542	2.63576e-03
RGWO	1.03165	3.12486	1.21082	829.35431	1.33865	2.44998e-03
JAYA	1.0307	3.4931	1.2014	1000	1.3514	2.42778e-03
STLBO	1.0305	3.4824	1.2013	982.0387	1.3511	**2.42507e-03**
TLABC	1.0305	3.4826	1.2013	982.1815	1.3512	**2.42507e-03**
CLPSO	1.0304	3.6131	1.1978	1000	1.3551	2.42806e-03
BLPSO	1.0305	3.5176	1.2002	992.7901	1.3522	2.42523e-03
DE/BBO	1.0303	3.6172	1.1969	1000	1.3552	2.42825e-03

Bold numbers are the best optimal answers

algorithm in the single, two, and three-diode models. It is noteworthy that the three-diode model is presented as being more accurate because it has a lower relative error value than the single- and two-diode models. The values of the five unknown parameters for the PWP201 solar module's single-diode model, which were determined using the DCSA algorithm in addition to 14 other algorithms, are displayed in Table 10.

The values of the five unknown parameters for the PWP201 solar module's single-diode model, which were determined using the DCSA algorithm in addition to 14 other algorithms, are displayed in Table 10. To ensure a thorough and equitable comparison, different techniques are also employed, such as JAYA [58], teaching–learning-based artificial bee colony (TLABC) [59], simplified teaching–learning-based optimization algorithm (STLBO) [60], comprehensive learning particle swarm optimizer (CLPSO) [61], biogeography-based learning particle swarm optimization (BLPSO) [54], and DE/BBO [62]. Examining Table 10 and comparing it with Table 5, it becomes evident that only the WHHO and SWOA methods achieved the lowest RMSE values. In addition, the STLBO and TLABC algorithms successfully attained a lower optimal value than that achieved by the other algorithms. When comparing algorithms, another crucial aspect is their convergence speed. Figure 11 graphically depicts the convergence speed over 5000 iterations of the algorithms. From this figure, it can be seen that the proposed method not only achieved the lowest RMSE value but also exhibited a faster convergence rate than the other algorithms.

Among the array of algorithms evaluated, the most efficient algorithm shows admirable performance when handling multiple unknown system parameters. Consequently, both two-diode and three-diode models are employed to allow for a more detailed investigation of these algorithms (see Tables 11 and 12). As it is clear from the tables, the algorithms that successfully obtained the lowest RMSE value in the single-diode model, such as the DCSA algorithm, did not show satisfactory performance with the increase in the number of unknown parameters. Figures 12 and 13 show the convergence speed of the algorithms in the two-diode and three-diode models and highlight the significant convergence speed of the DCSA algorithm. Of course, it should be noted that the CSA algorithm in the PWP201 system showed better performance compared to the French RTC system.

The strength and stability of algorithms shows another important aspect. Each algorithm was subjected to 30 executions and the results are summarized in Table 13. Based on this table, the DCSA algorithm exhibited exceptional performance, especially in the single diode model. In addition, SWOA and WHHO algorithms showed significant stability compared to other algorithms.

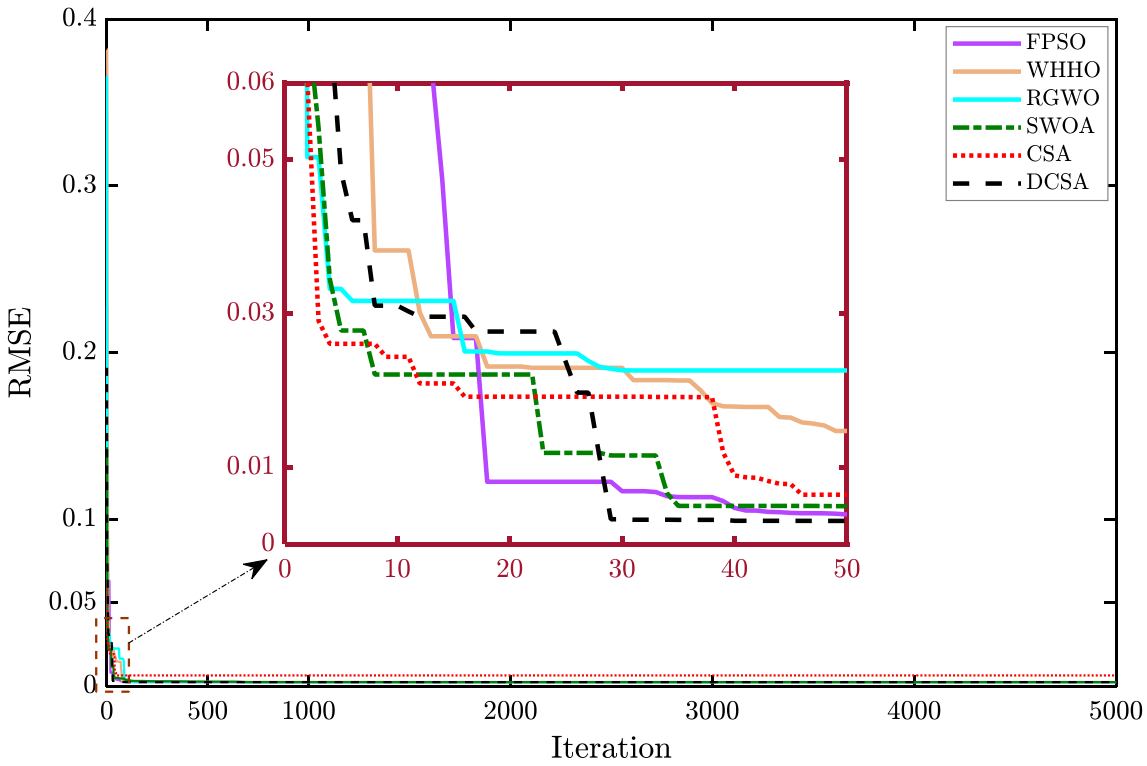

Fig. 11 Analysis of RMSE for algorithms in single diode model

Table 11 Detailed results for DDM of PWP201

Algorithm	$I_{ph}(A)$	$I_{sd1}(\mu A)$	$I_{sd2}(\mu A)$	$R_s(\Omega)$	$R_{sh}(\Omega)$	n_1	n_2	RMSE
DCSA	1.03242110	2.51278941	1.00001015	1.23910412	744.71214041	1.32004131	1.31720148	**2.04521e-03**
CSA	1.03051440	2.48223808	1.0000000	1.20127160	981.96741279	1.34999300	1.34998794	2.42507486e-03
FPSO	1.03060	2.4101	2.82452	1.20776	1000	1.94700	1.33105	2.48750e-03
WHHO	1.032381	2.51291	1.00005	1.23928	744.71538	1.31730	1.31693	2.04653e-03
EHHO	1.032341	2.67581	1.52821	1.23313	715.45241	1.54974	1.28392	2.2137e-03
SWOA	1.031434	2.63811	1.0001	1.23563	821.6525	1.32099	2.77788	2.0530e-03
CWOA	1.0332	2.6759	1.52820	1.23312	715.4537	1.5499	1.2844	2.2137e-03
WOA	1.0323	2.5129	1.0000	1.2392	744.7153	1.3173	1.3173	2.0465e-03
RGWO	1.03058	2.5126	2.91745	1.20717	1000	2	1.33376	2.48115e-03
JAYA	1.0326	2.6896	4.1973	1.2240	748.3831	1.3234	2.3680	2.2178e-03
STLBO	1.0328	2.5708	1.6899	1.2137	712.2977	1.3218	1.7314	2.2785e-03
TLABC	1.0331	2.6762	1.5280	1.2334	715.4478	1.5499	1.2832	2.2138e-03
CLPSO	1.0291	0.0010	9.3813	0.0314	75.6531	1.0000	1.5755	3.3925e-03
BLPSO	1.0265	9.2998	2.2586e-02	0.0301	1000	1.5225	1.4164	3.7559e-03
DE/BBO	1.0318	0.32774	2.4306e-06	1.2061	845.2495	1.3443	1.3443	2.400e-03

Bold numbers are the best optimal answers

Table 12 Detailed results for TDM of PWP201

Algorithm	$I_{ph}(A)$	$I_{sd1}(\mu A)$	$I_{sd2}(\mu A)$	$I_{sd3}(\mu A)$	$R_s(\Omega)$	$R_{sh}(\Omega)$	n_1	n_2	n_3	RMSE
DCSA	1.0305349	3.47164e-06	1.01010e-6	1.000000e-6	1.21021	985.3241	1.30153	1.866412	1.99995	2.0163e-03
CSA	1.03037	1.00000e-03	3.51252	1.00000e-6	1.2000	963.4851	1.9889	1.5214	1.95121	2.4560e-03
FPSO	1.03039	1.00000e-03	3.51253	1.00000e-6	1.20053	1000	2	1.35090	1.95841	2.42530e-03
WHHO	1.030514	3.48214e-06	1.000010e-6	1.000000e-6	1.200216	981.86961	1.39763	1.86704	2	2.0166e-03
EHHO	1.030571	3.439412	5.361479e-5	5.36524e-03	1.210242	991.362145	1.40361	1.40371	1.59847	2.4249e-03
SWOA	1.0305	3.4822e-06	1.0000e-6	1.0000e-6	1.2012	981.9781	1.4029	1.8671	2	2.0166e-03
CWOA	1.0305	3.4788	7.2209e-5	7.9930e-02	1.2005	992.7808	1.4032	1.9996	1.6487	2.4250e-03
WOA	1.0270	3.9028	2.0334e-4	6.0996e-02	1.1910	966.4183	1.4157	1.9992	1.6278	2.5814e-03
RGWO	1.030514	1	1.47299	1.00936	1.20126	982.02536	1.34999	1.34999	1.34999	2.42507e-03
JAYA	1.0263	2.4380	8.4019	2.4413e-01	1.1911	710.7260	1.3885	1.8790	1.3544	2.7525e-03
STLBO	1.0327	0	5.3435	2.4748	1.1448	1000	1.8457	1.4547	1.9590	3.4186e-03
TLABC	1.0264	9.1106	2.0912e-02	6.3249e-02	1.0869	602.9147	1.5220	1.3011	1.5370	3.7258e-03
CLPSO	1.0419	3.43995	6.6266e-07	35.1499	1	755.0178	1.9938	1.2982	1.9987	9.9858e-03
BLPSO	1.0344	4.7853	1.16444	2.6812e-03	1	1000	2	1.5566	2	6.3626e-03
DE/BBO	1.0307	0	3.2036	3.1737	1.1952	996.3251	1.7749	1.3965	1.9564	2.4916e-03

4.3 Experimental discussion

This section offers a discussion on the SM55, KC200GT, and SW255 solar modules, focusing on the parameters identified through the DCSA algorithm. Initially, the unknown parameters of these modules were determined under 1000 W/m2 irradiance and 25 °C, as presented in Table 14. Subsequently, Eqs. (11) and (12) were used to analyze the behavior of the identified model while considering temperature and irradiance variations. This investigation involves experiments at different temperatures and irradiance.

Figures 14, 15, and 16 correspond to SM55, KC200GT, and SW255 modules, respectively. These figures demonstrate that the experimental and identified models closely resemble each other with a negligible level of error that is inconsequential in engineering. Therefore, the accuracy of the parameters derived from the DCSA algorithm is convincingly established. These figures also show that as the irradiance decreases, the current produced by the solar module decreases, leading to a reduction in the power output.

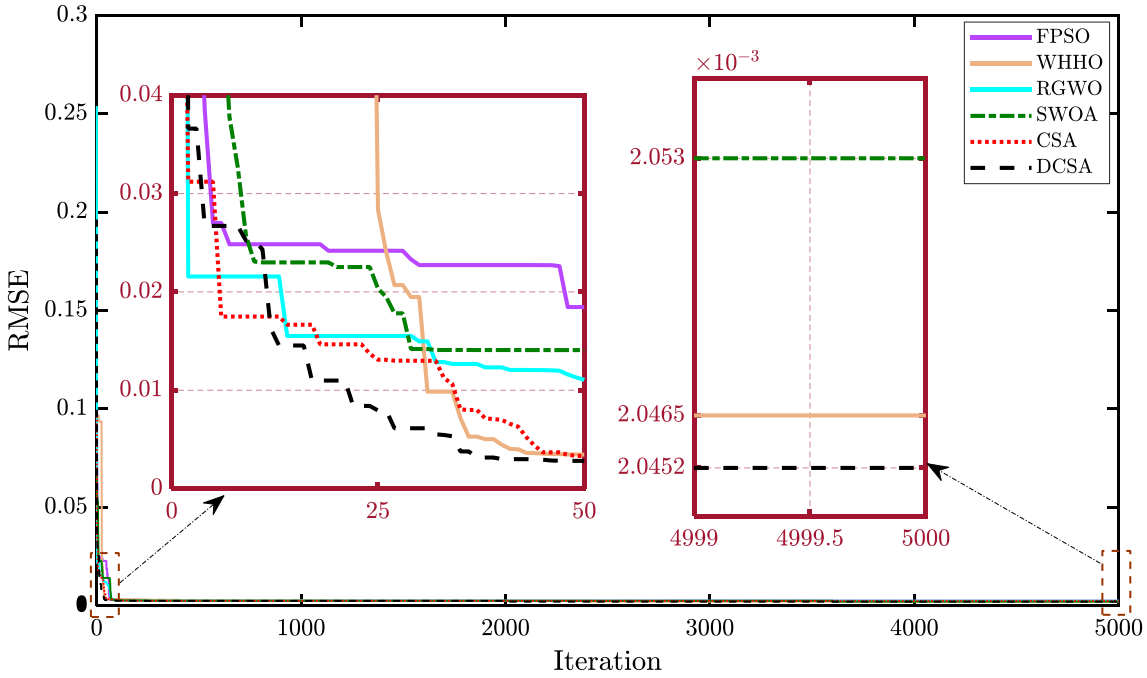

Fig. 12 Analysis of RMSE for algorithms in double diode model

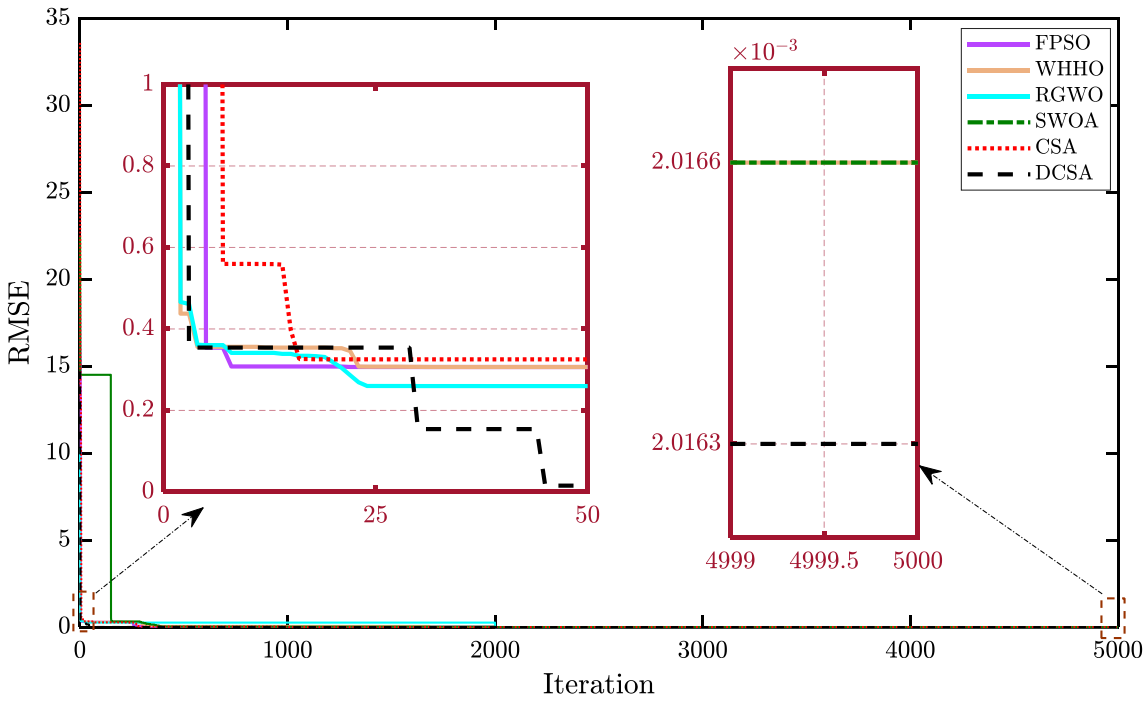

Fig. 13 Analysis of RMSE for algorithms in triple diode model

Figures 17 and 18 show the effect of temperature on SM55 and KC200GT modules, respectively. These figures provide further evidence that supports the accuracy of the parameters determined by the DCSA algorithm, as the observed behavior matches the experimental model. Particularly noteworthy is that these figures show how an increase in solar cell temperature corresponds to an increase in ohmic resistance, resulting in a decrease in current.

Table 13 Comparative evaluation of RMSE for SDM, DDM, and TDM of PWP201 through different methodologies over 30 runs

Algorithm	DCSA	CSA	FPSO	WHHO	EHHO	SWOA	CWOA	WOA	RGWO
SDM									
Min	**2.425074e-03**	6.43769589e-03	2.42525e-03	2.42507e-03	2.42516e-03	2.42507e-03	2.45168e-03	2.63576e-03	2.44998e-03
Mean	**2.425074e-03**	8.4671e-03	2.4252e-03	2.42510e-03	2.425669e-03	2.42507e-03	2.4678e-03	2.8476e-03	2.4597e-03
Max	**2.425074e-03**	1.0001e-02	2.4252e-03	2.4253e03	2.43125e-03	2.42507e-03	2.7864e-03	3.1647e-03	2.4949e-03
DDM									
Min	**2.04521e-03**	2.4250e-03	2.48750e-03	2.04653e-03	2.2137e-03	2.0530e-03	2.2137e-03	2.0465e-03	2.48115e-03
Mean	2.04550e-03	2.5364e-03	2.4895e-03	2.04887e-03	2.2264e-03	2.05464e-03	2.2647e-03	2.04774e-03	2.4889e-03
Max	2.04653e-03	2.5784e-03	2.4899e-03	2.5631e-03	3.1547e-03	2.05510e-03	2.8564e-03	2.4946e-03	2.4898e-03
TDM									
Min	**2.0163e-03**	2.4560e-03	2.42530e-03	2.0166e-03	2.4249e-03	2.0166e-03	2.4250e-03	2.5814e-03	2.42507e-03
Mean	2.0165e-03	2.7116e-03	2.4261e-03	2.02164e03	2.4316e-03	2.02146e-03	2.4251e-03	2.6154e-03	2.4251e-03
Max	2.0173e-03	2.7483e-03	2.4264e-03	2.03464e-03	2.4431e-03	2.06461e-03	2.4374e-03	2.8461e-03	2.4262e-03

Bold numbers are the best optimal answers

Table 14 Identification of Parameters for Three PV Modules using the WHHO Method at STC

Parameters	SM55	KC200GT	SW255
$I_{ph}(A)$	3.47247834	8.21647911	8.67132641
$I_{sd1}(\mu A)$	2.26431867e-02	0.00134211	0.16204862
$R_s(\Omega)$	0.32116455	0.23164712	0.12164795
$R_{sh}(\Omega)$	314.145134	754.115214	830.241762
n_1	1.00104792	1.05625013	1.21643871
RMSE	**2.04617912e-02**	**1.77341621e-02**	**1.44231401e-02**

Bold numbers are the best optimal answers

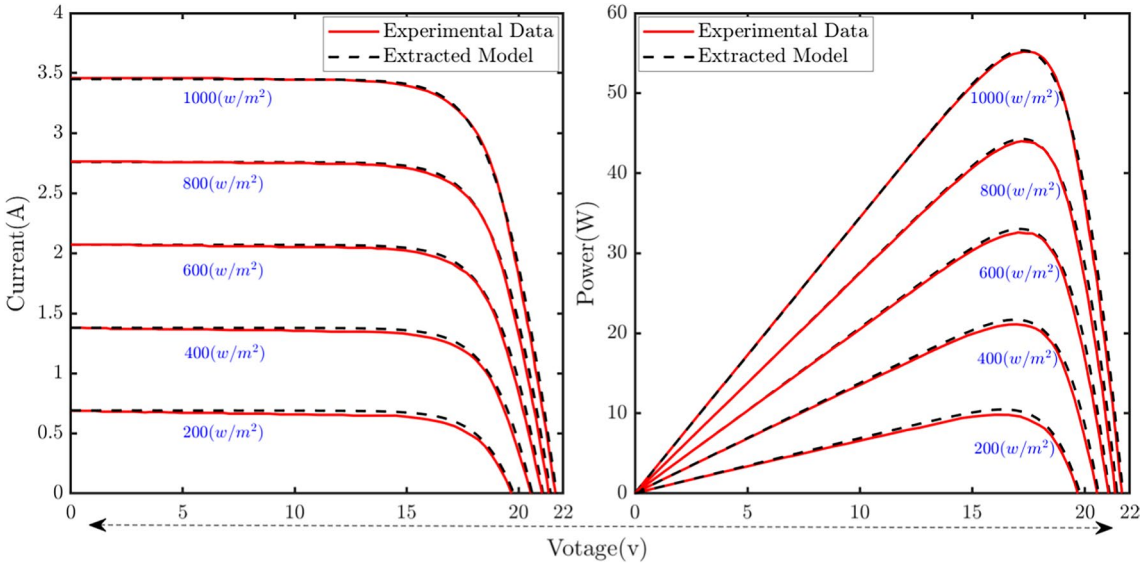

Fig. 14 Assessment of SM55 module characteristics: a comparison between parameters estimated by the proposed algorithm and manufacturer's specifications during irradiance fluctuations at a constant temperature of $T = 25°C$

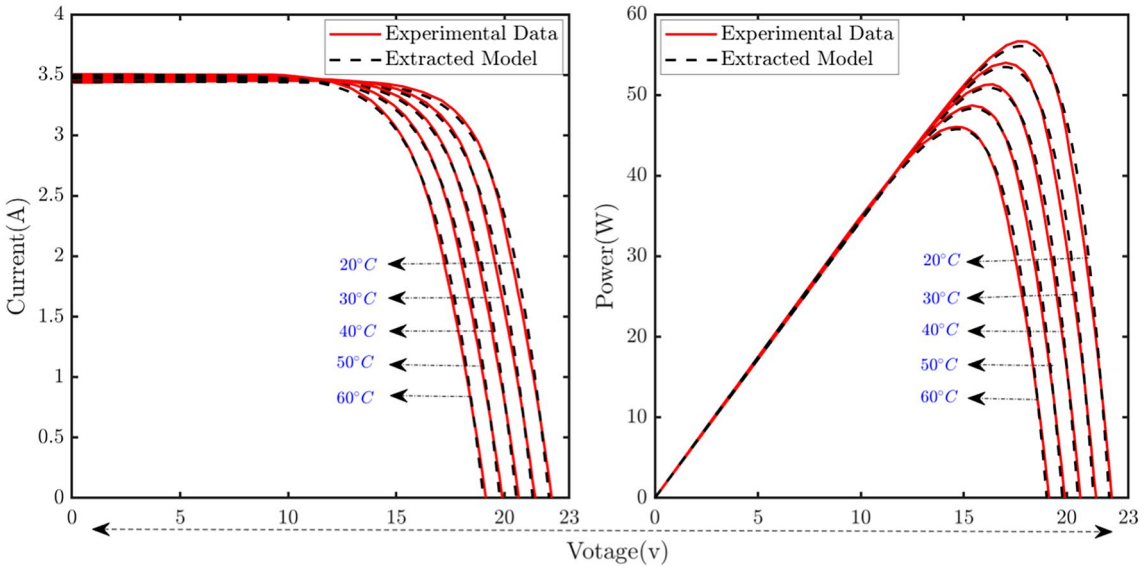

Fig. 15 Assessment of KC200GT module characteristics: comparing parameters estimated by proposed algorithm with manufacturer's specifications during irradiance fluctuations at constant $T = 25°C$

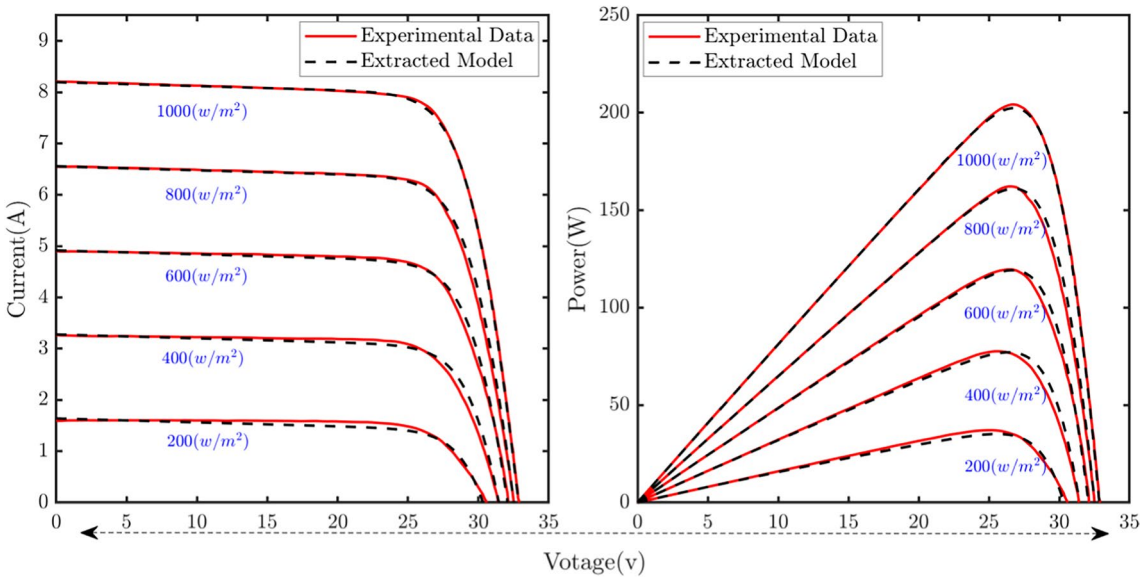

Fig. 16 Assessment of SW255 module features using proposed algorithm compared to manufacturer's specifications under variable irradiance at constant temperature of $T = 25°C$

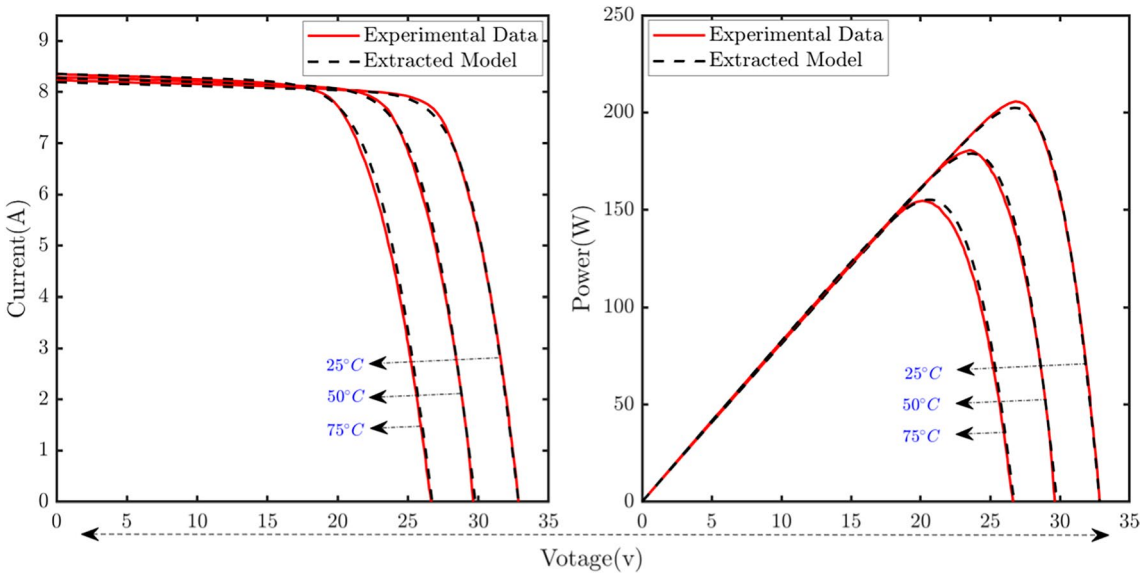

Fig. 17 Assessment of SM55 module characteristics: comparative analysis of parameters estimated by the proposed algorithm versus manufacturer's specifications during temperature variations at constant irradiance $G = 1000^{W}/_{m^2}$

4.4 The module parameters as a function of temperature and irradiance

In this section, we examine the effect of temperature and radiation on the parameters of the mathematical model of the solar cell. Based on the previous section, where a direct correlation was established between the radiation and current produced by the solar cell, as well as an inverse relationship between temperature and current, we further confirm these connections through the results presented in Tables 15 and 16. Table 16 clearly shows that with the temperature remaining constant at 25 °C, radiation intensification results in a proportional increase in current source (I_{ph}), while the shunt resistance (R_{sh}), series resistance (R_s), and diode ideality factor (n_1) remain relatively stable. In addition, the reverse saturation current (I_{sd1}) of the diode exhibits a direct relationship with temperature, leading to an augmented absorption of photons as the temperature increases. As a result, the value of I_{sd1} also increased, as shown in Table 16.

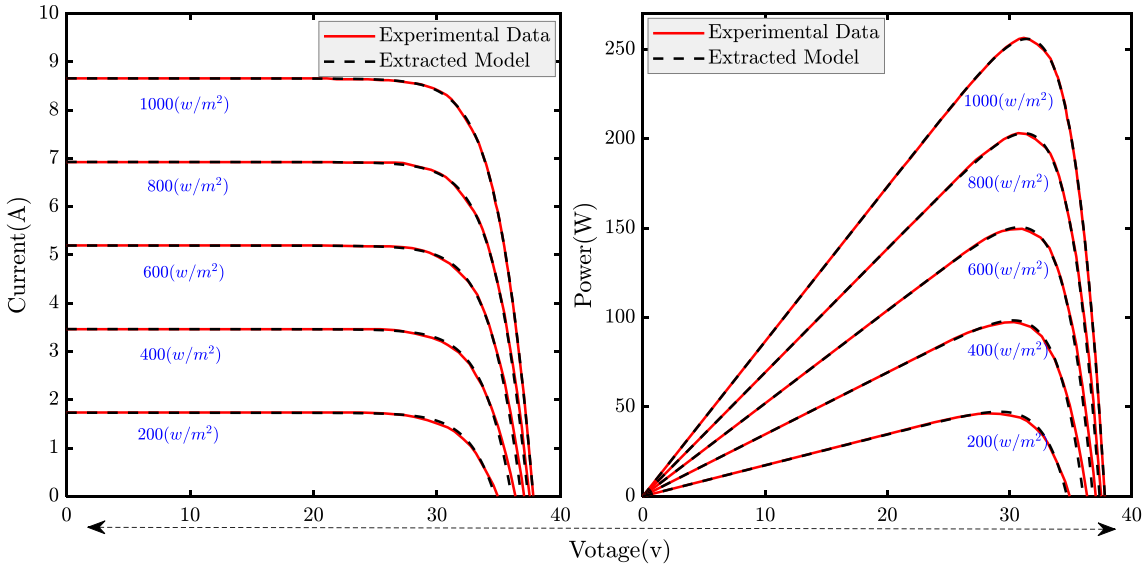

Fig. 18 Assessment of KC200GT module characteristics: a comparative analysis of parameters estimated by the proposed algorithm versus manufacturer's specifications across temperature variations at constant irradiance $G = 1000^{W}/_{m^2}$

Furthermore, the series resistance value (R_s) consistently falls below 0.4, which confirms that the series resistance value for monocrystalline modules is always less than 0.4. Moreover, the ideal coefficient of the diode, represented by n_1, varies across different modules. For example, the emission-type KC200GT module exhibits an ideal coefficient of n that is almost equal to 1.

5 Conclusions

In this study, we successfully introduced and validated a novel method that significantly enhances the performance of metacognitive algorithms, particularly during the exploitation and exploration phases. By integrating this method into the Crow Search Optimization Algorithm, we addressed its deficiencies in convergence speed, robustness, stability, and ability to escape local minima. The resulting Diligent Crow Search Optimization Algorithm (DCSA) demonstrated remarkable improvements, including a 98% increase in stability and a sevenfold acceleration in convergence speed. The application of the DCSA to solar cell parameter identification further underscored its efficacy, achieving optimal power output across various solar cell models and panels under different conditions. These results highlight the method's potential to address critical global challenges in solar energy optimization.

Future research can extend the application of this method to other metaheuristic algorithms, such as the grasshopper algorithm, to enhance their performance in similar contexts. This study paves the way for broader adoption and further innovation in the field of metaheuristic algorithm optimization.

Table 15 WHHO-derived optimal parameter estimates for three types of PV modules across varying irradiance (G) levels and a constant temperature of $T = 25°C$

Parameters	SM55	KC200GT	SW255
G = 200			
$I_{ph}(A)$	0.67154796	1.60131461	1.73217946
$I_{sd1}(\mu A)$	0.02132465	4.85120347e-04	0.03134230
$R_s(\Omega)$	0.31625391	1.10009874	0.38241631
$R_{sh}(\Omega)$	3.49120e + 02	9.13301467e + 02	9.8536472e + 02
n_1	1.020413275	1.010347621	1.27014621
RMSE	**2.11047e-02**	**7.62149e-03**	**9.31461e-03**
G = 400			
$I_{ph}(A)$	1.38120411	3.25678412	3.47167943
$I_{sd1}(\mu A)$	3.05341e-04	0.00769436	0.02316249
$R_s(\Omega)$	0.71014627	0.43314657	0.25016317
$R_{sh}(\Omega)$	3.39001e + 02	1.37131469e + 02	9.98346170e + 02
n_1	1.0100	1.10101346	1.231647901
RMSE	**6.61625e-03**	**1.36149731e-02**	**1.2301629e-02**
G = 600			
$I_{ph}(A)$	2.07614973	4.87694292	5.2023105
$I_{sd1}(\mu A)$	2.71031460e-04	0.06314622	0.0098465
$R_s(\Omega)$	0.323164721	0.27501341	0.2025876
$R_{sh}(\Omega)$	3.4523791e + 02	4.0116794e + 02	1000
n_1	1	1.1001346	1.1924671
RMSE	**9.31612e-03**	**4.0130951**	**1.721408e-02**
G = 800			
$I_{ph}(A)$	2.76231491	6.55416792	6.9331462
$I_{sd1}(\mu A)$	4.471264e-04	4.231345e-04	0.0121308
$R_s(\Omega)$	0.32397461	0.3212301	0.14921561
$R_{sh}(\Omega)$	3.3136798e + 02	1.4815631e + 02	9.68314e + 02
n_1	1.02213098	1	1.20612369
RMSE	**1.31469e-02**	**2.713657e-02**	**2.519463e-02**
G = 1000			
$I_{ph}(A)$	3.4531698	8.211236498	8.6713064
$I_{sd1}(\mu A)$	2.376413e-04	0.00156440	0.0165149
$R_s(\Omega)$	0.41364703	0.24136479	0.1213247
$R_{sh}(\Omega)$	3.4323210e + 02	1.302236e + 02	9.251421e + 02
n_1	1	1.0513642	1.2121468
RMSE	**2.031064e-02**	**2.87136e-02**	**9.674913e-03**

Bold numbers are the best optimal answers

Table 16 WHHO-Derived Optimal Parameter Estimates for Three Modules Across Varied Temperature Conditions under a Constant Irradiance of $G = 1000^{W}/_{m^2}$

PV modules	Temperature	$I_{ph}(A)$	$I_{sd1}(\mu A)$	$R_s(\Omega)$	$R_{sh}(\Omega)$	n_1	**RMSE**
	20°C	3.4513647	5.55e-04	0.516594	435.364721	1.086497	**1.7061e-02**
	30°C	3.4415146	0.0083207	0.489437	432.255146	1.145373	**2.16352e-02**
SM55	40°C	3.4369743	1.0136452	0.4511642	466.701042	1.308491	**1.56106e-02**
	50°C	3.4313210	0.0986423	0.4823049	330.630153	1.133026	**1.5164e-02**
	60°C	3.4352501	1.0011206	0.4551469	466.653741	1.216491	**1.79431e-02**
	25°C	8.2153164	0.0013846	0.248468	1.302194e + 02	1.155146	**2.7469e-02**
KC200GT	50°C	8.2098736	3.7719562	0.1551469	3.210146e + 02	1.465641	**8.16494e-02**
	75°C	8.2051264	3.556824	0.2525479	2.46013e + 02	1.309463	**4.92146e-02**

Bold numbers are the best optimal answers

Author contributions M.J. and M.N. wrote the main manuscript, Data curation, Software, Methodology,, M.Z and L.T Writing—review & editing, Writing—original draft, S.P Project administration, Supervision, J.V.Q.Data curation, Software, Supervision, Methodology,

Data availability The datasets generated during and/or analyzed during the current study are available from the corresponding author on reasonable request.

Declarations

Competing interests The authors declare no competing interests.

References

1. Arandian B, Eslami M, Khalid SA, Khan B, Sheikh UU, Akbari E, Mohammed AH. An effective optimization algorithm for parameters identification of photovoltaic models. IEEE Access. 2022;10:34069–84.
2. Jabari M, Rad A, Nasab MA, Zand M, Padmanaban S, Muyeen SM, Guerrero JM. Parameter identification of PV solar cells and modules using bio dynamics grasshopper optimization algorithm. IET Gener Transm Distrib. 2024. https://doi.org/10.1049/gtd2.13279.
3. Afrand M, Shahsavar A, Sardari PT, Sopian K, Salehipour H. Energy and exergy analysis of two novel hybrid solar photovoltaic geothermal energy systems incorporating a building integrated photovoltaic thermal system and an earth air heat exchanger system. Sol Energy. 2019;188:83–95.
4. Tyagi VV, Rahim NA, Rahim NA, Jeyraj A, Selvaraj L. Progress in solar PV technology: research and achievement. Renew Sustain Energy Rev. 2013;20:443–61.
5. Bendaoud R, Amiry H, Benhmida M, Zohal B, Yadir S, Bounouar S, Hajjaj C, Baghaz E, El Aydi M. New method for extracting physical parameters of PV generators combining an implemented genetic algorithm and the simulated annealing algorithm. Sol Energy. 2019;194:239–47.
6. Ebrahimi SM, Rezaie B, Tavan M. Identification of the three-axis pedestal using Euler-Lagrange method using mathematical approach. Int J Model Ident Control. 2023;42(3):211–25.
7. Chenouard R, El-Sehiemy RA. An interval branch and bound global optimization algorithm for parameter estimation of three photovoltaic models. Energy Convers Manage. 2020;205:112400.
8. Al-Masri HM, Magableh SK, Abuelrub A. Output power computation and sizing of a photovoltaic array by advanced modeling. Sustain Energy Technol Assess. 2021;47:101519.
9. Al-Masri HM, Magableh SK, Abuelrub A, Alzaareer K. Realistic coordination and sizing of a solar array combined with pumped hydro storage system. J Energy Storage. 2021;41:102915.
10. Al-Masri HM, Magableh SK, Abuelrub A, Saadeh O, Ehsani M. Impact of different photovoltaic models on the design of a combined solar array and pumped hydro storage system. Appl Sci. 2020;10(10):3650.
11. Ebrahimi SM, Norouzi F, Dastres H, Faieghi R, Naderi M, Malekzadeh M. Sensor fault detection and compensation with performance prescription for robotic manipulators. J Franklin Inst. 2024;361(7):106742.
12. Qais MH, Hasanien HM, Alghuwainem S. Parameters extraction of three-diode photovoltaic model using computation and Harris Hawks optimization. Energy. 2020;195:117040.
13. Ridha HM, Hizam H, Mirjalili S, Othman ML, Ya'acob ME, Ahmadipour M. Novel parameter extraction for Single, Double, and three diodes photovoltaic models based on robust adaptive arithmetic optimization algorithm and adaptive damping method of Berndt-Hall-Hall-Hausman. Sol Energy. 2022;243:35–61.
14. Sulyok G, Summhammer J. Extraction of a photovoltaic cell's double-diode model parameters from data sheet values. Energy Sci Eng. 2018;6(5):424–36.
15. Xiong G, Zhang J, Shi D, He Y. Parameter extraction of solar photovoltaic models using an improved whale optimization algorithm. Energy Convers Manage. 2018;174:388–405.
16. Muhsen DH, Ghazali AB, Khatib T, Abed IA. Parameters extraction of double diode photovoltaic module's model based on hybrid evolutionary algorithm. Energy Convers Manage. 2015;105:552–61.
17. Nayak B, Mohapatra A, Mohanty KB. Parameter estimation of single diode PV module based on GWO algorithm. Renew Energy Focus. 2019;30:1–12.
18. Bastidas-Rodriguez JD, Petrone G, Ramos-Paja CA, Spagnuolo G. A genetic algorithm for identifying the single diode model parameters of a photovoltaic panel. Math Comput Simul. 2017;131:38–54.
19. Olabi AG, Rezk H, Abdelkareem MA, Awotwe T, Maghrabie HM, Selim FF, Rahman SMA, Shah SK, Zaky AA. Optimal parameter identification of perovskite solar cells using modified bald eagle search optimization algorithm. Energies. 2023;16(1):471.

20. Dastres H, Ebrahimi SM, Malekzadeh M, Gordillo F. Robust adaptive parameter estimator design for a multi-sinusoidal signal with fixed-time stability and guaranteed prescribed performance boundary of estimation error. J Franklin Inst. 2023;360(1):223–50.
21. Alghamdi MA, Khan MFN, Khan AK, Khan I, Ahmed A, Kiani AT, Khan MA. PV model parameter estimation using modified FPA with dynamic switch probability and step size function. IEEE Access. 2021;9:42027–44.
22. Ye X, Liu W, Li H, Wang M, Chi C, Liang G, Chen H, Huang H. Modified whale optimization algorithm for solar cell and PV module parameter identification. Complexity. 2021;2021:1–23.
23. Aldosary A, Ali ZM, Alhaider MM, Ghahremani M, Dadfar S, Suzuki K. A modified shuffled frog algorithm to improve MPPT controller in PV System with storage batteries under variable atmospheric conditions. Control Eng Pract. 2021;112:104831.
24. SetayeshNazar M. Optimal placement of fixed series compensation and phase shifting transformer in the multi-year generation and transmission expansion planning problem at the pool-based market for maximizing social welfare and reducing the investment costs. IET Gener Transm Distrib. 2022;16(15):2959–76.
25. Guo L, Meng Z, Sun Y, Wang L. Parameter identification and sensitivity analysis of solar cell models with cat swarm optimization algorithm. Energy Convers Manage. 2016;108:520–8.
26. Kumar C, Raj TD, Premkumar M, Raj TD. A new stochastic slime mould optimization algorithm for the estimation of solar photovoltaic cell parameters. Optik. 2020;223:165277.
27. Jervase JA, Bourdoucen H, Al-Lawati A. Solar cell parameter extraction using genetic algorithms. Meas Sci Technol. 2001;12(11):1922.
28. Alam DF, Yousri DA, Eteiba MB. Flower pollination algorithm based solar PV parameter estimation. Energy Convers Manage. 2015;101:410–22.
29. Subudhi B, Pradhan R. Bacterial foraging optimization approach to parameter extraction of a photovoltaic module. IEEE Trans Sustain Energy. 2017;9(1):381–9.
30. Yang B, Wang J, Zhang X, Yu T, Yao W, Shu H, Zeng F, Sun L. Comprehensive overview of meta-heuristic algorithm applications on PV cell parameter identification. Energy Convers Manage. 2020;208:112595.
31. Rezk H, Olabi AG, Wilberforce T, Sayed ET. A comprehensive review and application of metaheuristics in solving the optimal parameter identification problems. Sustainability. 2023;15(7):5732.
32. Premkumar M, Jangir P, Ramakrishnan C, Nalinipriya G, Alhelou HH, Kumar BS. Identification of solar photovoltaic model parameters using an improved gradient-based optimization algorithm with chaotic drifts. IEEE Access. 2021;9:62347–79.
33. Wu Z, Yu D, Kang X. Parameter identification of photovoltaic cell model based on improved ant lion optimizer. Energy Convers Manage. 2017;151:107–15.
34. Askarzadeh A, dos Santos Coelho L. Determination of photovoltaic modules parameters at different operating conditions using a novel bird mating optimizer approach. Energy Convers Manage. 2015;89:608–14.
35. Abdelminaam DS, Said M, Houssein EH. Turbulent flow of water-based optimization using new objective function for parameter extraction of six photovoltaic models. IEEE Access. 2021;9:35382–98.
36. Jiao S, Chong G, Huang C, Hu H, Wang M, Heidari AA, Chen H, Zhao X. Orthogonally adapted Harris hawks optimization for parameter estimation of photovoltaic models. Energy. 2020;203:117804.
37. Pourmousa N, Ebrahimi SM, Malekzadeh M, Alizadeh M. Parameter estimation of photovoltaic cells using improved Lozi map based chaotic optimization Algorithm. Sol Energy. 2019;180:180–91.
38. Jiang LL, Maskell DL, Patra JC. Parameter estimation of solar cells and modules using an improved adaptive differential evolution algorithm. Appl Energy. 2013;112:185–93.
39. Ebrahimi SM, Salahshour E, Malekzadeh M, Gordillo F. Parameters identification of PV solar cells and modules using flexible particle swarm optimization algorithm. Energy. 2019;179:358–72.
40. Yaghoubi M, Eslami M, Noroozi M, Mohammadi H, Kamari O, Palani S. Modified salp swarm optimization for parameter estimation of solar PV models. IEEE Access. 2022;10:110181–94.
41. Gupta J, Nijhawan P, Ganguli S. Parameter extraction of solar PV cell models using novel metaheuristic chaotic tunicate swarm algorithm. Int Trans Electr Energy Syst. 2021;31(12):e13244.
42. Gao X, Cui Y, Hu J, Xu G, Wang Z, Qu J, Wang H. Parameter extraction of solar cell models using improved shuffled complex evolution algorithm. Energy Convers Manage. 2018;157:460–79.
43. Naeijian M, Rahimnejad A, Ebrahimi SM, Pourmousa N, Gadsden SA. Parameter estimation of PV solar cells and modules using Whippy Harris Hawks optimization algorithm. Energy Rep. 2021;7:4047–63.
44. Pourmousa N, Ebrahimi SM, Malekzadeh M, Gordillo F. Using a novel optimization algorithm for parameter extraction of photovoltaic cells and modules. Eur Phys J Plus. 2021;136(4):470.
45. Ebrahimi SM, Hasanzadeh S, Khatibi S. Parameter identification of fuel cell using repairable grey Wolf optimization algorithm. Appl Soft Comput. 2023;147:110791.
46. Ebrahimi SM, Malekzadeh M, Alizadeh M, HosseinNia SH. Parameter identification of nonlinear system using an improved Lozi map based chaotic optimization algorithm (ILCOA). Evol Syst. 2021;12:255–72.
47. Salahshour E, Malekzadeh M, Gordillo F, Ghasemi J. Quantum neural network-based intelligent controller design for CSTR using modified particle swarm optimization algorithm. Trans Inst Meas Control. 2019;41(2):392–404.
48. Salahshour E, Malekzadeh M, Gholipour R, Khorashadizadeh S. Designing multi-layer quantum neural network controller for chaos control of rod-type plasma torch system using improved particle swarm optimization. Evol Syst. 2019;10:317–31.
49. Rastegar S, Araújo R, Malekzadeh M, Gomes A, Jorge H. A new NIALM system design based on neural network architecture and adaptive springy particle swarm optimization algorithm. Energ Effi. 2023;16(6):1–17.
50. Taleshian T, Malekzadeh M, Sadati J. Parameters identification of photovoltaic solar cells using FIPSO-SQP algorithm. Optik. 2023;283:170900.
51. Omar A, Hasanien HM, Elgendy MA, Badr MA. Identification of the photovoltaic model parameters using the crow search algorithm. J Eng. 2017;2017(13):1570–5.
52. Easwarakhanthan T, Bottin J, Bouhouch I, Boutrit C. Nonlinear minimization algorithm for determining the solar cell parameters with microcomputers. Int J Solar Energy. 1986;4(1):1–12.

53. Reddy SS, Yammani C. A novel two step method to extract the parameters of the single diode model of Photovoltaic module using experimental Power-Voltage data. Optik. 2021;248:167977.
54. Nourizadeh H, Nazar MS. Customer-oriented scheduling of active distribution system considering integrated demand response programs and multi-carrier energy hubs. J Clean Prod. 2024;447:141308.
55. Yıldıran N, Tacer E. Identification of photovoltaic cell single diode discrete model parameters based on datasheet values. Sol Energy. 2016;127:175–83.
56. Chaibi Y, Salhi M, El-Jouni A, Essadki A. A new method to extract the equivalent circuit parameters of a photovoltaic panel. Sol Energy. 2018;163:376–86.
57. Askarzadeh A. A novel metaheuristic method for solving constrained engineering optimization problems: crow search algorithm. Comput Struct. 2016;169:1–12.
58. Rao R. Jaya: a simple and new optimization algorithm for solving constrained and unconstrained optimization problems. Int J Ind Eng Comput. 2016;7(1):19–34.
59. Chen X, Xu B, Mei C, Ding Y, Li K. Teaching–learning–based artificial bee colony for solar photovoltaic parameter estimation. Appl Energy. 2018;212:1578–88.
60. Niu Q, Zhang H, Li K. An improved TLBO with elite strategy for parameters identification of PEM fuel cell and solar cell models. Int J Hydrogen Energy. 2014;39(8):3837–54.
61. Liang JJ, Qin AK, Suganthan PN, Baskar S. Comprehensive learning particle swarm optimizer for global optimization of multimodal functions. IEEE Trans Evol Comput. 2006;10(3):281–95.
62. Gong W, Cai Z, Ling CX. DE/BBO: a hybrid differential evolution with biogeography-based optimization for global numerical optimization. Soft Comput. 2010;15:645–65.
63. Diab AAZ, Sultan HM, Do TD, Kamel OM, Mossa MA. Coyote optimization algorithm for parameters estimation of various models of solar cells and PV modules. Ieee Access. 2020;8:111102–40.
64. Mostafa M, Rezk H, Aly M, Ahmed EM. A new strategy based on slime mould algorithm to extract the optimal model parameters of solar PV panel. Sustain Energy Technol Assess. 2020;42:100849.
65. Rezk H, Babu TS, Al-Dhaifallah M, Ziedan HA. A robust parameter estimation approach based on stochastic fractal search optimization algorithm applied to solar PV parameters. Energy Rep. 2021;7:620–40.
66. Heshmatollah N, et al. Insulation Life Estimation of Low Voltage Self-Supporting XLPE Cables Installed in Electric Power Distribution Network of Ilam Province, Iran: A Case Study in Ilam Province Electric Power Distribution Company. 2023 27th International Electrical Power Distribution Networks Conference (EPDC). IEEE, 2023.
67. El-Fergany AA. Parameters identification of PV model using improved slime mould optimizer and Lambert W-function. Energy Rep. 2021;7:875–87.
68. Singla MK, Nijhawan P. Triple diode parameter estimation of solar PV cell using hybrid algorithm. Int J Environ Sci Technol. 2021. https://doi.org/10.1007/s13762-021-03286-.
69. Gafar M, El-Sehiemy RA, Hasanien HM, Abaza A. Optimal parameter estimation of three solar cell models using modified spotted hyena optimization. J Ambient Intell Humaniz Comput. 2022. https://doi.org/10.1007/s12652-022-03896-9.
70. El-Dabah MA, El-Sehiemy RA, Hasanien HM, Saad B. Photovoltaic model parameters identification using an innovative optimization algorithm. IET Renew Power Gener. 2023;17(7):1783–96.